Georg Wilding, BSc

Linearity and residual dose correction of a LiF:Mg,Ti thermoluminescence dosimeter

MASTER THESIS

For obtaining the academic degree
Diplom-Ingenieur

Master Programme of
Technical Physics

Graz University of Technology

Supervisor:
Assoc.Prof. Dipl.-Phys. Dr.rer.nat. Wolfgang Sprengel
Institute of Materials Physics

in cooperation with:
Seibersdorf Labor GmbH

Graz, February 2015

EIDESSTATTLICHE ERKLÄRUNG

AFFIDAVIT

Ich erkläre an Eides statt, dass ich die vorliegende Arbeit selbstständig verfasst, andere als die angegebenen Quellen/Hilfsmittel nicht benutzt, und die den benutzten Quellen wörtlich und inhaltlich entnommenen Stellen als solche kenntlich gemacht habe. Das in TUGRAZonline hochgeladene Textdokument ist mit der vorliegenden Masterarbeit/Diplomarbeit/Dissertation identisch.

I declare that I have authored this thesis independently, that I have not used other than the declared sources/resources, and that I have explicitly indicated all material which has been quoted either literally or by content from the sources used. The text document uploaded to TUGRAZonline is identical to the present master's thesis/diploma thesis/doctoral dissertation.

_____ _____

Datum / Date Unterschrift / Signature

Acknowledgement

First of all, I would like to thank my supervisor Dr. Wolfgang Sprengel for all the helpful input and experience he could provide.

I am also very grateful for Dr. Hannes Stadtmann's helpful support with the experiments I conducted at Seibersdorf Labor GmbH, as well as for the many inspiring discussions. As my supervisor at Seibersdorf, his practical advice was of great value.

My parents and my brother have supported me throughout my studies, for which I am incredibly grateful.

And most of all I would like to thank my girlfriend, for her loving support and constant encouragement.

Abstract

Thermoluminescence dosimetry makes use of the thermoluminescent properties of certain materials. These materials store the energy of incident ionising radiation and release it again as light when heated. The emitted amount of light is largely proportional to the irradiated dose. An example for such a material is lithium fluoride doped with magnesium and titanium (abbreviated as LiF:Mg,Ti and commonly known under the label TLD-100), which is used at Seibersdorf Labor GmbH in the personal routine dosimetry programme. Three challenges arise when working with TLD-100: The first one is caused by slightly varying production conditions, which lead to a different zero-dose of every dosimeter. The second challenge occurs in connection with irradiations of high doses, which cause a residual dose to be imprinted on the dosimeter and disturb further measurements. The third is the effect of supralinearity, which leads to disproportionately large doses to be calculated for incident doses above a certain threshold. The aim of this study is to model the influences of these properties and to correct and improve the dose calculation, both at low doses of few μGy and at high doses of several Gy.

Table of Contents

1. Introduction

Radiation and in particular ionising radiation occurs in a wide range of fields, covering medical applications in diagnosis via X-ray computer tomography, in treatments via radiotherapy, industrial applications for defect control of materials and food sterilisation. However, the occurrence of ionising radiation is of course not always intentional: the recent disaster in the Fukushima Daiichi nuclear plant is a striking example of the problematic side of ionising radiation. All these examples, whether in the deliberate use of ionising radiation or not show that radiation protection is necessary. Radiation protection is crucial for medical personal who execute an X-ray scan as well as for the workers at a nuclear plant. To allow appropriate protection, the extent of radiation exposure needs to be known. Therefore, collected and monitored data must be as accurate as possible. This is the aim of dosimetry.

The amount of ionising radiation (the dose) can be measured for a person at the workplace (personal dosimetry) or in a certain location (environmental dosimetry). Even though there is a variety of ways to achieve this, an increasingly frequent one is utilising the thermoluminescent properties of certain materials. These materials store the energy of incident ionising radiation for a certain amount of time and release the energy in the form of light once the material is heated. The amount of light emitted can be recorded and used to calculate the dose stored on the dosimeter containing the thermoluminescent crystal.

For this study the properties of a thermolumenescent material made of lithium fluoride doped with magnesium and titanium (abbreviated as LiF:Mg,Ti) were investigated. The thermoluminescence dosimeter in question is labeled TLD-100 and is used by Seibersdorf Labor GmbH for routine dosimetry. This study will investigate the relation of the emitted light and the irradiated dose, its proportionality and linearity. Thermoluminescence dosimeters have several advantages, such as low production costs, small size and mass, a quick and easy to automise readout process and a wide dose range. However, the usage is accompanied by several limitations and problems, which will be targeted in this study.

The first problem is caused by the production process and the fact that different production batches of crystals exhibit slightly different behaviour when reading out the dosimeters. This leads to a slightly different *zero-dose* of every dosimeter. This dose of an unirradiated dosimeter is of the order of several μGy, which is roughly 10 % of the dose from the natural background accumulated during one month and therefore mainly of interest when dealing with very low doses.

The second problem arises when a dosimeter is subjected to a very high dose. This has a long-term influence on the crystal as it, sometimes significantly, increases the zero-dose. This additional dose is termed *residual dose* and its reduction, possible elimination and correction, as well as its cause are among the primary concerns of this thesis as well as in the practical application in the routine dosimetry programme at Seibersdorf Labor GmbH.

The third problem also occurs at high doses and is an effect called *supralinearity*. This effect

causes the measurement of disproportionately large doses when dosimeters are irradiated with doses greater than 1 Gy. A way to correct this for the TLD-100 will be devised.

All three problems cause a more or less strong deviation from a perfect linear behaviour. Whereas the zero-dose and the residual dose have the strongest influence at low to medium doses, the supralinearity only affects measurements of high doses. For a thorough investigation it is therefore necessary to be able to irradiate a wide range of doses. This is facilitated by the possibility to carry out irradiations directly in facilities at the Seibersdorf research centre.

The details of the procedures are the subject of this thesis. The necessary theory concerning thermoluminescence and the processes behind it are treated in chapter 2. Chapter 3 discusses the basics of radiation, radiation protection and dosimetry. The equipment and facilities that were used are described in chapter 4. Information concerning data acquisition, such as the irradiations that were carried out, the corresponding measurements and additional data provided by Seibersdorf Labor GmbH, is also treated in chapter 4. Emphasis is placed on the linearity and supralinearity of the TLD-100 and ways to decrease or, if this should not be possible, quantise the residual dose to improve measurements. This is analysed in chapter 5. Thus, the ultimate aim is to apply the derived method for the routine dosimetry programme in Seibersdorf.

2. Theory of Thermoluminescence

2.1. Effects of Luminescence

Certain crystals can store energy and release it again at a later stage. The name of these crystals also hints at the way in which this energy can be released: thermoluminescent crystals, for example, release the stored energy when heated (thermo-) by emitting light (-luminescent).

The term thermoluminescence was coined in the year 1895 by Wiedemann and Schmidt (1895), though the effect was already known much earlier: in 1664 Robert Boyle achieved to make a diamond emit light using candles as well as body heat (Boyle, 1664). The stored energy can also be released in other forms, depending on the material. Furthermore, different materials can store different forms of energy. Therefore, there are two ways to classify them: One focuses on what is caused by heating the crystal, whereas the other highlights the source of the stored energy. The first class encompasses processes known as "Thermally Stimulated Phenomena" (McKeever et al., 1995) which are all (as the name suggests) caused by heating. Among these are for example:

- Thermally Stimulated Conductivity,
- Thermally Stimulated Polarisation,
- Thermally Stimulated Capacitance, and
- Thermally Stimulated Luminescence (Thermoluminescence).

Table 2.1 gives examples of the second class which refers to processes that excite the crystal so that light can be emitted later (McKinlay, 1981).

Effect	Excitation
Chemiluminescence	Chemical energy
Triboluminescence	Mechanical energy
Sonoluminescence	Acoustic energy
Radioluminescence	Ionising radiation

Table 2.1.: Effects of luminescence and the corresponding cause of the excitation.

The most important means of excitation among these is ionising radiation. A thermoluminescent crystal allows incoming ionising radiation to be stored in the material and later, when heated, to be released again in the form of light. The emitted light can easily be recorded

and, furthermore, used to calculate the amount of ionising radiation, the dose, which makes an application for dosimetry possible. This aspect of luminescence is the primary focus of this work as well as the investigation of the relation between the irradiated dose and the measured luminosity.

Following the common use in literature, throughout this thesis the term *thermoluminescence* is used in the sense of *thermally stimulated radioluminescence*.

The whole process can be divide into three phases:

1. Absorption: Incoming ionising radiation is absorbed by the crystal.
2. Storage: The energy of this radiation is stored within the crystal.
3. Release: By heating, the stored energy is released.

The duration of the second phase can vary strongly and calls for a third differentiation: the process is called *fluorescence* when the storage time (or lifetime) is less than $10^{-8}\,\mathrm{s}$ or *phosphorescence* when it is larger than a few seconds (Chen and McKeever, 1997).

2.2. General Process

In the first phase, ionising radiation in the form of a photon is absorbed by the crystal. The energy of the radiation must be converted into a, by the crystal, storable form. This happens by transfering energy to electrons which are then excited into higher energy levels. From the excited level, an electron can decay directly back to the ground state, which is the before mentioned *fluorescence*. If, however, the electron is trapped at a metastable state or energy level, the time between the absorption of the photon from the ionising radiation and the emission of the (thermoluminescent) photon can be much longer. These processes are depicted in Figure 2.1.

Starting at the ground level (A) the electron gets excited by an incoming photon to the excited level (B). From there it can decay back to the ground level straight away (2a) or may be trapped at a metastable level (C). It remains there for a certain amount of time, for example until the material is heated and the necessary activation energy to release the electron is provided. This energy moves it back to the excited state (3) wherefrom it decays back to the ground state, again releasing energy in the form of a photon.

The metastable levels are also called trapping centres or traps and correspond to defects in the material.

2.3. Mathematical Models

2.3.1. A first-order Model of Thermoluminescence

The duration of the electrons remaining trapped in the metastable state depends on the temperature (as heating can release electrons) and on the energy difference between the metastable level C and the excited level B, the activation energy. Randal and Wilkinson already formulated a theory describing this in 1945 (Randall and Wilkins, 1945a). Their so

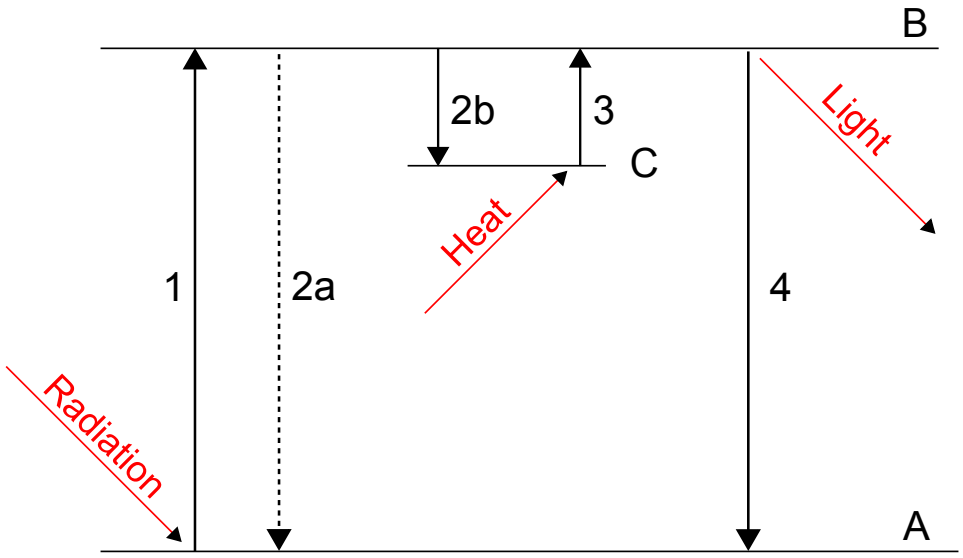

Figure 2.1.: Energy levels in thermoluminescence. First (1) the electron is excited from the ground level A to the excited level B. From there it can decay to the ground level again (2a) or may be trapped in a metastable level C (2b). If released from the metastable state it moves again to the excited state (3) wherefrom it decays back to ground level again (4).

called first-order model is based on an exponential model of excitation from the metastable level C to the excited level B and a following decay into the ground state. The Arrhenius equation 2.1 gives the probability p for an electron to move from C up to B. This probability is basically a Boltzmann distribution caused by a Maxwellian energy distribution of the trapped electrons.

$$p = se^{-\frac{E}{k_B T}} \tag{2.1}$$

Here, k_B is the Boltzmann constant, s is a constant frequency factor depending on the metastable state C, E is the activation energy of that state and T the temperature. This probability is converted to a "rate of release of electrons from the trap" (McKinlay, 1981), given in equation 2.2.

$$-\frac{dn}{dt} = nse^{-\frac{E}{k_B T}} \tag{2.2}$$

This equation indicates how many electrons can escape the trap (per unit time), depending on activation energy E, temperature T, number of electrons n in C and the constant s. The higher the activation energy, i.e., the deeper the trap and the lower the temperature, the fewer electrons can escape. This makes it possible to increase the temperature and to release the stored electrons in a controlled way.

Taking equation 2.2 one can calculate the intensity of the emitted light at a certain temperature. Equation 2.3 (McKinlay, 1981) gives an expression for the glow intensity,

calculated by integrating over equation 2.2.

$$I(T) \propto ns \exp\left(-\frac{E}{k_B T}\right) \exp\left(-\int_{T_0}^{T} \frac{s}{R} \exp\left(-\frac{E}{k_B \xi}\right) \mathrm{d}\xi\right) \tag{2.3}$$

Here, s is again the material constant, E is the activation energy, R is the heating rate, k_B is the Boltzmann constant and T_0 is the starting temperature. $I(T)$ gives the intensity emitted by a trap at a certain temperature T. For various temperatures T increasing with R the graph $I(T)$ is known as the glow curve. However, $I(T)$ is not the intensity of the emitted light itself, but rather an amount of electrons released from a trap, which can of course be *related* to the emitted light. The intensity of simulated glow curves in this thesis is therefore usually given normalised and in arbitrary units. It is also the reason calibration is necessary when working with thermoluminescence dosimeters. Figure 2.2 gives an example simulated according to equation 2.3. At the beginning of the heating phase the intensity increases exponentially until it reaches the maximum, the glow peak. At higher temperatures the intensity decreases again and reaches zero eventually. All electrons have now been removed from the trap which is again empty.

As mentioned earlier, a trap or metastable state corresponds to a defect in the crystal structure. In the presented model the activation energy E together with the parameter s are parameters specific to the defect. As there is always a large number of different defects in a crystal, several combinations of parameters appear, leading to the appearance of different peaks in the glow curve. The example given in figure 2.2 was calculated with just one defect type whereas for the calculation of the glow curve shown in figure 2.3 six different sets of parameters were used. They correspond to the defects found in LiF:Mg,Ti, which are discussed in detail in section 2.5.1. Usually, the population of electrons in the traps and with it the size of the peaks in the glow curve is determined by the amount of incident radiation. For the simulation of this glow curves the populations were set to arbitrary units to resemble real glow curves.

2.3.2. A second-order Model of Thermoluminescence

In section 2.3.1 it was assumed that electrons released from the trap always decay to the ground state, meaning that no retrapping occurs. Randall and Wilkins (1945b) argue that this retrapping not impossible, but merely unlikely. In an advanced model by Garlick and Gibson (1948) it is therefore considered that electrons can be retrapped again (at the same or at a different trapping centre). This is now termed a second-order model where the equations are slightly different compared to the first-order model.

The rate of release of electrons from the trap is given by equation 2.4. The exponential remains the same as in the corresponding equation of the first-order model, but the pre-factor is now dependent on the total trap concentration N. Here, n is again the concentration of trapped electrons, E the activation energy, k_B the Boltzmann constant and T the temperature.

$$-\frac{dn}{dt} = \frac{n^2 s}{N} e^{-\frac{E}{k_B T}} \tag{2.4}$$

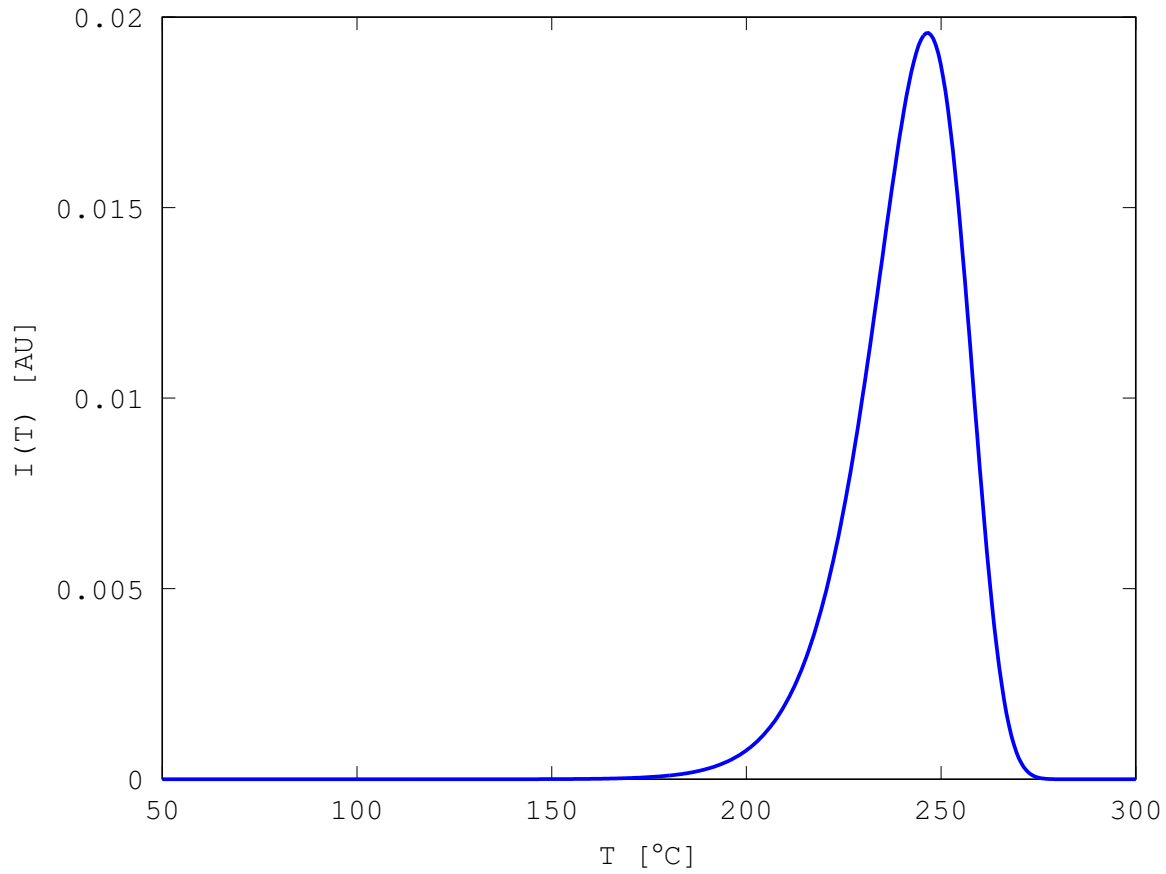

Figure 2.2.: A glow curve calculated according to equation 2.3 with a heating rate of 1 Ks^{-1} and one defect. The intensity I (in arbitrary units) is dependent on the temperature T. The activation energy E of the corresponding trap is 1.93 eV and the material constant s is $5.22 \cdot 10^{18}\,s^{-1}$. This trap corresponds to peak 5 in the glow curve of the material LiF:Mg,Ti and is discussed in more detail later in section 2.5.1).

Integrating this equation again gives an expression for the emitted intensity at temperature T.

$$I(T) \propto n_0^2 \frac{s}{N} \exp\left(-\frac{E}{k_B T}\right)\left[1 + \frac{ns}{RN} \exp\left(-\int_{T_0}^{T} \frac{s}{R} \exp\left(-\frac{E}{k_B \xi}\right) \mathrm{d}\xi\right)\right]^{-2} \tag{2.5}$$

Both, the here mentioned second-order model and the before mentioned first-order model, are based on actual physical processes. Another model, the so called general-order model by May and Partridge (1964), is a purely empirical one, and, although it produces glow curves that correspond to measured ones, it does not relate to the actual processes (Pagonis et al., 2006).

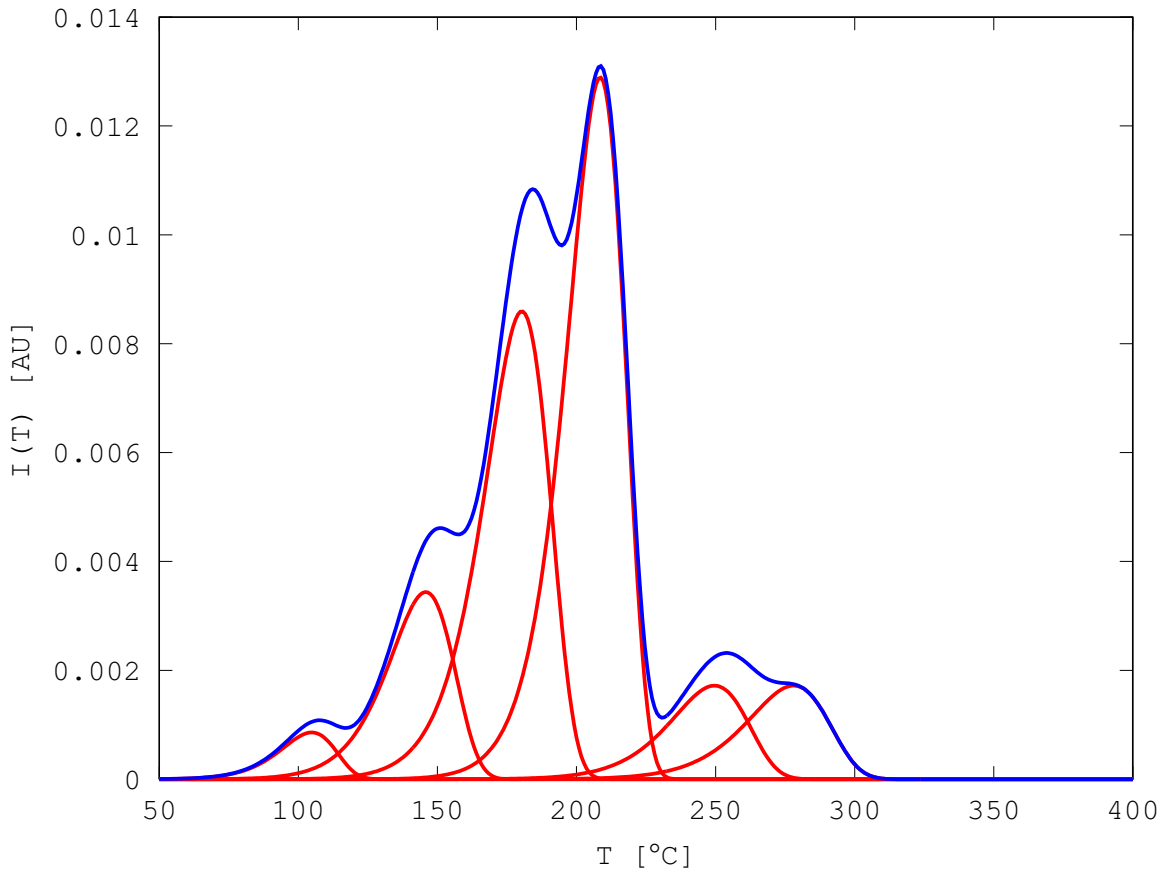

Figure 2.3.: A glow curve calculated according to equation 2.3 with a heating rate of 30 Ks^{-1} and six defects. The glow curves of the different traps (red) simply add up to the total glow curve (blue). The activation energies E_k of the corresponding traps and the material constants s_k correspond to the peaks in LiF:Mg,Ti and are given in table 2.5.

2.4. Thermoluminescent Materials

A wide range of materials show thermoluminescent properties. Following McKeever et al. (1995) a classification in 4 families or material classes is recommended. This ranges from fluorides, including the now widely used lithium fluoride (LiF) in several variations, over oxides (a prominent one being aluminium oxide) to sulphates and borates. A short description shall be given here, with the focus put on the fluorides. A general overview over several more important materials and their properties is given in table 2.2.

2.4.1. Fluorides

Among the fluorides lithium flouride (LiF) was one of the first materials investigated with thermoluminescent properties. Research dates back to at least 1952 when it was investigated

by Morehead and Daniels (1952) and it is by now widely used in different compositions with different dopants. The two most prominent varieties used are LiF doped either with magnesium and titanium (LiF:Mg,Ti) or with magnesium, copper and phosphor (LiF:Mg,Cu,P). Of these LiF:Mg,Ti is the older one dating back to the 60s, with patents granted in 1963 and 1967, (McKeever et al., 1995) and is today most commonly used for dosimetry. The compound LiF:Mg,Cu,P is a more recent development and has a much higher sensitivity compared to LiF:Mg,Ti.

The dosimeter used for this thesis is made of LiF:Mg,Ti and produced by Thermo Scientific under the tradename TLD-100 (TLD stands for *thermoluminescence dosimeter*). The version doped with magnesium, copper and phosphor is called TLD-100H. This technically is a manufacturer naming, though LiF:Mg,Ti is also in literature usually called TLD-100. Table 2.2 gives a summary of the most important materials, including the different commercial names given to them.

A big advantage of all LiF materials is the tissue-equivalence of the effective atomic number Z_{eff} which is 7.4 for soft tissue (because of the water content) and 8.2 for TLD-100 (see Table 2.3 for other Z_{eff} values of different materials).

Composition	Li isotope	Thermo Scientific	TLD Poland
LiF:Mg,Ti	natural	TLD-100	MTS-N
LiF:Mg,Ti	Li-6 enriched	TLD-600	MTS-6
LiF:Mg,Ti	Li-7 enriched	TLD-700	MTS-7
LiF:Mg,Cu,P	natural	TLD-100H	MCP-N
LiF:Mg,Cu,P	Li-6 enriched	TLD-600H	MCP-6
LiF:Mg,Cu,P	Li-7 enriched	TLD-700H	MCP-7
CaF_2:Dy	-	TLD-200	-
CaF_2:Mn	-	TLD-400	-
Al_2O_3:C	-	TLD-500	-
$Li_2B_4O_2$:Mn	natural	TLD-800	-
$CaSO_4$:Dy	-	TLD-900	-

Table 2.2.: List of TLD materials and their designation by the two manufacturers Thermo Scientific (Thermo Fisher Scientific Inc., 2007) and TLD Poland (TLD Poland, 2015). Where lithium is present in the compound the isotopic composition is given (for a detailed composition see table 2.4).

Isotopic composition

Another possible variation is which isotopic composition is used for lithium, with TLD-100 using natural lithium whereas TLD-600 is enriched in Li-6 and TLD-700 enriched in Li-7. The advantage of a different isotopic composition is that it enables detection of neutrons, which cannot be done with TLD-100(H). These detect only β- and γ-radiation. Table 2.4 gives the detailed composition (McKeever et al., 1995) and the areas of usage (Thermo Fisher Scientific Inc., 2007).

Name	Range	Z_{eff}	Sensitivity	Fading
TLD-100	10 μGy - 10 Gy	8.2	1	5%/year
TLD-600	10 μGy - 10 Gy	8.2	1	5%/year
TLD-700	10 μGy - 10 Gy	8.2	1	5%/year
TLD-100H	1 μGy - 10 Gy	8.2	15	negligible
TLD-600H	1 μGy - 10 Gy	8.2	15	negligible
TLD-700H	1 μGy - 10 Gy	7.4	15	negligible
TLD-200	0.1 μGy - 10 Gy	16.3	30	16%/2 weeks
TLD-400	0.1 μGy - 100 Gy	16.3	10	12%/2 weeks
TLD-500	0.05 μGy - 1 Gy	10.2	30	3%/year
TLD-800	0.5 mGy - 100 kGy	7.4	0.15	5%/3 months
TLD-900	1 μGy - 100 Gy	15.5	20	8%/6 months

Table 2.3.: Detailed values for different TLD materials of the manufacturer Thermo Scientific (Thermo Fisher Scientific Inc., 2007). The sensitivity is given relative to TLD-100.

Type	Li-6 content	Li-7 content	Application
TLD-100(H)	7.5%	92.5%	Health and medical physics
TLD-600(H)	95.6%	4.4%	Neutron dosimetry
TLD-700(H)	0.06%	99.93%	Gamma/beta dosimetry

Table 2.4.: Different isotope composition for TLD-100, TLD-600 and TLD-700 (McKeever et al., 1995). It applies also for the H series doped with magnesium, copper and phosphor.

Production

These TLD materials can be produced in a wide variety of forms, from small rods to circular or quadratic chips. For this study, the dosimeters contain TLD-100 in the form of small chips with a size of 3.2x3.2 mm^2 and a thickness of 0.38 mm. For the production of these chips usually a crystal is grown which is then ground into a powder and pressed or sintered into the desired form. This production produces defects which on one hand contribute to the thermoluminescence but on the other hand also produce differences between different batches of chips. This is one of the reasons why a calibration has to be done before using a TL dosimeter.

Calcium fluoride

Calcium fluoride also exhibits thermoluminescent properties and is used either doped with dysprosium (CaF_2:Dy) and called TLD-200 or doped with manganese (CaF_2:Mn), called TLD-400. Both have a higher Z_{eff} than soft tissue and are primarily used for environmental dosimetry.

2.4.2. Other Materials

Other classes of thermoluminescent materials that are used for dosimetry are oxides, sulphates and borates. All are used for dosimeters produced by Thermo Scientific, examples are TLD-500 (aluminium oxide doped with carbon), TLD-900 (calcium sulphate doped with dysprosium) or TLD-800 (a borate). TLD-500 and 900 have a higher Z_{eff} than TLD-100 and are mainly used in environmental dosimetry, whereas TLD-800 has a low sensitivity and is used for dosimetry with high doses.

2.5. Role of Defects

The trapping of the excited electrons occurs at lattice defects. There are three types of lattice defects (McKinlay, 1981):

1. Intrinsic defects
2. Extrinsic defects
3. Defects caused by ionising radiation

All three types of defects contribute to the effect of thermoluminescence though the importance varies with the material in question.

Intrinsic defects would also appear in a (hypothetically) pure crystal where lattice atoms are for example displaced and occupy an interstitial position in the lattice (Frenkel defect) or, in the case of an ionic crystal, when a pair, i.e., an anion and a cation, are missing entirely (Schottky defect).

Extrinsic defects are caused by doping the crystal with small amounts of a different material. For example, the dosimeter used in this study (the TLD-100 made of LiF:Ti,Mg) is composed of a lithium fluoride lattice and is doped with small amounts of titanium and magnesium.

The third type of lattice defects are defects caused by irradiation. The electrons stored at one of the first two defects fall in this category as well as lattice atoms displaced by radiation (McKeever et al., 1995).

In addition to figure 2.1, where the process of thermoluminescence is viewed from the perspective of the energy states, a second model is possible, given in figure 2.4. This incorporates the creation of electron-hole pairs where the holes get trapped similarly to the electrons.

In figure 2.4 incoming radiation creates an electron-hole pair (e^- and h^+ respectively, bottom left corner) in the valence band. They can either recombine straight away (corresponding to a decay back to the ground state according to figure 2.1) or seperate. If they separate they can move through the crystal, the electron in the conduction band C and the hole in the valence band V. Both can be trapped at metastable states, either at electron traps (E_T) or hole traps (H_T) and remain trapped there for a certain time. They can be released when the necessary activation energy is provided in the form of heat. This process also happens spontaneously if the trap is shallow. Hole traps for example are rather unstable

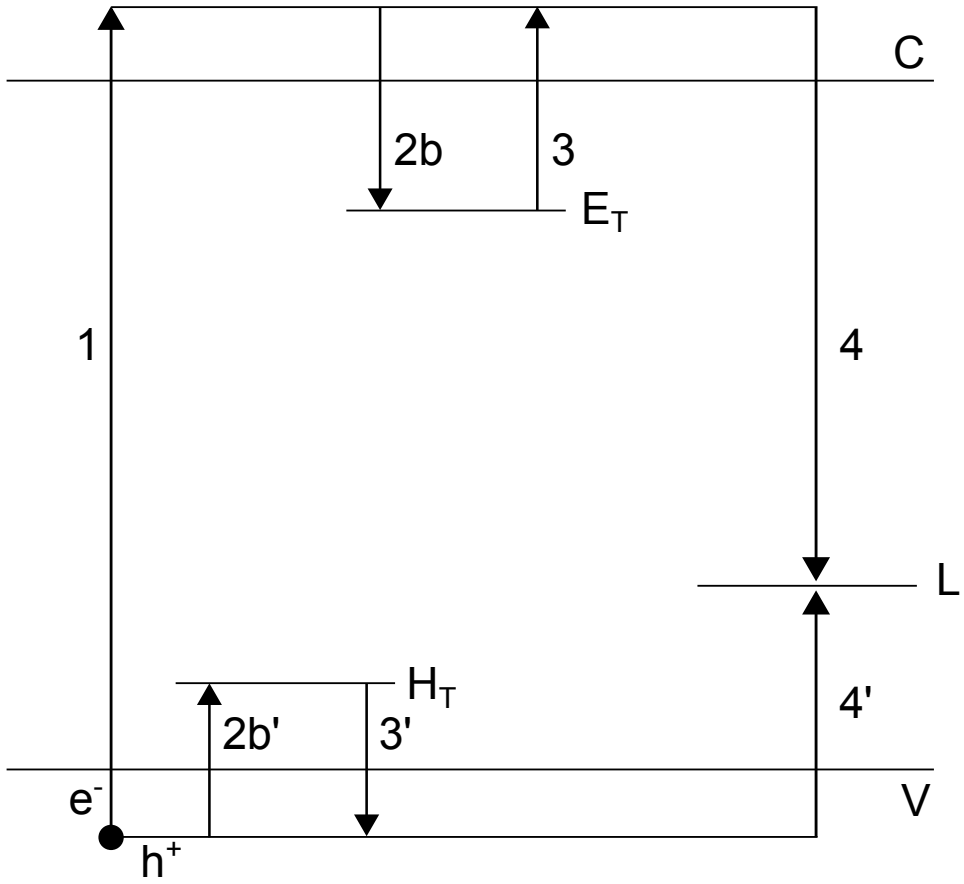

Figure 2.4.: Schematic of the energy bands, including both electrons and holes. The upper part of the diagram is equivalent to figure 2.1, the bottom part depicts the process for holes. The electron-hole pair is created at the bottom left corner and then seperated, with the electron (e^-) changing into the conduction band C and the hole (h^+) into the valence band V. There exist both hole traps and electron traps, E_T and H_T, respectively. Hole traps are rather unstable at room temperature and quickly release holes again (McKinlay, 1981). After the release, electrons and holes can either be retrapped again or recombine at a luminescence centre L while emitting light or a recombination centre (not shown in diagram) without emitting light.

at room temperature and quickly release holes again (McKinlay, 1981). Once released they move on until they are either trapped again or reach a luminescence centre L, where they recombine and emit light. If recombination happens at a centre without emitting light the corresponding centre is called a recombination centre.

2.5.1. Defects of TLD-100

The crystal structure of LiF, the main component of the TLD-100, is face centred cubic, made of Li^+ and F^-. The two main defects are Schottky defects, where both a Li^+ and a F^- ion are missing, and Frenkel defects, where a Li^+ or a F^- are moved from a lattice position to an interstitial position. The dopants in TLD-100 are magensium and titanium.

Magnesium enters the lattice as Mg^{2+} and substitutes for a Li^+ atom. As charge neutrality has to be kept, this happens in combination with the appearence of a Li^+ vacancy (written as Mg-Li_{vac}). Through coulombic interaction between the positively charged Mg^{2+} ions and the negatively charged vacancies they form pairs, so called dipoles (Strutt and Lilley, 1981). To minimise the free energy these dipoles in turn combine, forming higher order clusters, especially trimers, where 3 dipoles cluster together (McKeever and Lilley, 1982). Appart from clustering the formation of stable or metastable precipitates is possible (Bradbury and Lilley, 1977). This precipitates decrease the sensitivity whereas it is increased by clusters. The ratio between clusters and precipitates determines the thermoluminescent properties of a material and is itself strongly dependant on temperature during and cooling rate after production (Bos et al., 1992).

Titanium also enters the lattice by replacing a Li^+ atom. As it can be either Ti^{3+} or Ti^{4+} there are several ways to reach charge neutrality, for example as $TiOH_n$ complexes (Stoebe and DeWerd, 1985). Whereas these complexes increase the thermoluminescent behaviour, the OH^- appearing in the latter also forms $MgOH_m$ complexes which decrease the emitted thermoluminescence. It was suggested by Wachter (1982) that this happens because $MgOH_m$ complexes form centres competing with luminescence centres. This means that OH^- can have an TL increasing or TL decreasing effect, depending on the concentration. Common concentrations are 180-200 ppm Mg and 10 ppm Ti, along with several ppm OH^- (Wachter, 1982).

As mentioned earlier, an important factor, during production as well as during usage, is the temperature. There exist various methods of annealing, either before usage and irradiation, after irradiation or before readout which will increase the sensitivity and enable better measurements. In most cases the duration, the temperature and the cooling rate is adjusted to improve the thermoluminescent properties (Bos et al., 1992).

The different defects mentioned here give rise to different glow peaks, and not all defects are completeley understood with the research still going on. A method to determine peak properties is for example by investigating the optical absorption characteristics (Oster and Horowitz, 2010), where absorption bands appear at certain energies. These can be correlated to certain peaks of the glow curve. The second peak, for example, is connected to a Mag-Li_{vac} dipole and the fifth peak to a Mag-Li_{vac} trimer.

Trapping parameters

There are several traps in the material TLD-100, and not all of them are important for the application in dosimetry. Table 2.5 gives a list of 7 important traps or peaks in the glow curve together with the activation energy and the lattice constant (Stadtmann et al., 2002; Fairchild et al., 1978). These parameters vary depending on the source because on one hand

different batches of the same material yield slightly different results and on the other varying measurement and treatment parameters, such as annealing temperatures and the heating rate, also have an influence on the parameters s and E. Furthermore, peaks 3 and 5 are sometimes, depending on the application and the way the parameters are calculated, split into two peaks each.

Peak	E [eV]	s [s^{-1}]
1	1.04	$1 \cdot 10^{15}$
2	1.24	$1.14 \cdot 10^{15}$
3	1.30	$1.45 \cdot 10^{14}$
4	1.52	$2.6 \cdot 10^{15}$
5	1.93	$5.22 \cdot 10^{18}$
6	1.70	$1 \cdot 10^{15}$
7	1.79	$1 \cdot 10^{15}$

Table 2.5.: Trap parameters of TLD-100. The parameters of peaks 2-5 are taken from Stadtmann et al. (2002), while the paramters of peaks 1, 6 and 7 are taken from Fairchild et al. (1978). It should be noted that the peak parameters vary between different publications. The reason is that they strongly depend on the model and the method with which they are calculated.

2.5.2. Fading

An important effect is fading, which means the decrease of stored information in a TL material over time. From the first-order model it is possible to derive a formula for the half-life by solving the differential equation 2.2. This yields:

$$t_{\frac{1}{2}} = \frac{\ln 2}{s} e^{\frac{E}{k_B T}} \tag{2.6}$$

However, the half-lives calculated with this formula differ from experimental values (table 2.6), suggesting that other processes are also at work (Bos, 2001).

Table 2.3 gives the different fading values provided by the manufacturer for the materials mentioned. The fading is of course temperature dependent, as the probability of releasing an electron from a trap is higher if the temperature is higher (see equation 2.1). As mentioned before, there are several traps in the material corresponding to different defects and usually with different activation energies. Traps with low activation energies can be seen as shallow traps where the temperature needed to release an electron is rather low. This causes shallow traps to be emptied already at room temperature, at least to a significant amount. Table 2.6 lists the half-lives of the prominent peaks in TLD-100 (McKinlay, 1981).

The low half-lives of peaks 1 and 2 mean that these will basically be empty as electrons stored in the traps are continuously released again. The half-life of 3 months of peak 3 means that about 80 % of the energy is still stored after one month of application. This is problematic as the TLD-100 is routinely worn for one month and then read out. However,

Peak	Half-life
1	10 min
2	1 day
3	3 months
4	8.5 years
5	80 years
6	several hundred years

Table 2.6.: Half-lifes of different traps in TLD-100 at room temperature (McKinlay, 1981).

this can be easily corrected by simply preheating the dosimeters at a low temperature before the actual heating in the readout procedure and thus emptying trap 3. The long half-lives of peaks 4 and 5 make them suitable for use in dosimetry, as they are very stable.

2.6. Linearity/Supralinearity

As mentioned before, the emitted light is used to calculate the dose the material was exposed to. The amount of light emitted has to be correlated to a dose, usually by a linear function or a factor, as it is not possible to directly calculate the absorbed dose from the emitted light. How this can be done and the different methods that exist are described later in section 3.5.1. That the relation between the amount of stored energy and the dose is linear is in fact only an assumption, which of course does not hold for every material. Nevertheless, materials used in dosimetry are usually required to have linear properties at least over a certain range of absorbed doses.

A way to quantify the linearity of a material (or in the applied sense of a dosimeter) is the supralinearity index $f(D)$, first introduced by Horowitz (1981) and Mische and McKeever (1989):

$$f(D) = \frac{S(D)/D}{S(D_1)/D_1} \tag{2.7}$$

Here $S(D)$ is the calculated or measured dose value at an irradiated dose D. The denominator is calculated from an arbitrarily selected dose in the linear range. This causes $f(D)$ to be 1 when it is calculated within this linear range (as nominator and denominator are then equal). Supralinearity occurs at doses where $f(D) > 1$ and a disproportionately high dose is calculated, while $f(D) < 1$ signifies a saturated or sublinear region where a smaller than irradiated dose is calculated. Linear or supralinear behaviour is always defined in relation to a reference point, which, for an easier application, is placed in the linear range.

TLD-100 has a linear range of up to several Gy, followed by a supralinear region. The saturated region starts at about 1000 Gy. Not all materials exhibit all of these regions, the TLD-100H for example has no supralinear region at all. Above all, the definition of the supralinearity index is only possible if the material in question has a linear range where the fraction $\frac{S(D_1)}{D_1}$ can be defined.

There are two basic possibilities for where the source of the supralinearity lies:

- During irradiation, where energy is stored by exciting electrons, or
- during readout, where the material is heated and the stored energy is released.

Accordingly, the two respective theories are called *Competition during excitation* and *Competition during heating*. They shall be described here briefly, followed by an adapted and more recent model which includes competition during heating as well as a track interaction model that connects supralinearity with the ionisation density.

2.6.1. Competition During Excitation

Competition during excitation means that the excess in emitted thermoluminescence is already caused during the excitation phase. The basic principle is that there are two competing traps during irradiation that can store electrons, but only one of them is responsible for the emitted thermoluminescence. It is assumed that less electrons can be trapped at the competing trap while the probability of trapping an electron is at the same time higher. This causes more electrons to be stored at the trap connected to thermoluminescence once the competing trap is full, which in turn leads to the increase in emitted thermoluminescence called supralinearity.

2.6.2. Competition During Heating

The excess in emitted thermoluminescence is assumed to be caused during the heating phase when the filled traps are emptied. Here, only one trap and one recombination (or luminescence) centre are considered. The emitted luminescence is determined by the filling of the trap (n) and the recombination centre (m), which in turn are proportional to the dose D. Depending on the irradiated dose the luminescence is either proportional to the minimum of n and m or the product of n and m. In the first case it is therefore also proportional to D whereas in the second case it is proportional to D^2.

2.6.3. Unified Interaction Model (UNIM)

Because the filling and emptying of traps cannot be observed directly a model combining competition during heating and excitation is necessary. This was investigated by Chen and Fogel (1993), who developed a model where both competition during excitation and competition during heating are realised. Their simulations showed however that supralinearity mainly stems from competition during heating.

This is supported by other models which also incorporate dose-rate and ionisation density, additionally to competition during heating. One of these is the unified track/defect interaction model (UNIM), which was first devised in the 90s (Horowitz et al., 1996). It connects the supralinear behaviour of LiF:Mg,Ti with the significantly different ionisation density of α- and γ-radiation. The reason is the different location where recombinations occur during

the heating phase. In the case of heavy charged particles (HCP) intra-track recombination (recombination within the ionisation path) is of greater importance at low doses and causes a linear dose response, whereas inter-track recombination (recombination between different tracks) becomes more important at high doses and leads to supralinear behaviour. A similar process occurs with γ-irradiation, where linear behaviour is caused by interaction within the trapping/luminescence centre and supralinear behaviour by charge carrier migration at high doses.

Therefore, similar processes cause the respective linear or supralinear behaviour. At low doses and with few ionisation tracks recombinations occur mostly within the track (intra-track recombination). With increasing dose levels the distance between the tracks decreases and with it the efficiency of competition centres. This increases the luminescence efficiency and leads to supralinear behaviour.

Up to now, the UNIM is still being used as it allows to model the properties of supralinearity better than previous models, for example by taking the overlapping tracks of incident particles into account (Lavon et al., 2015).

2.7. Zero-dose

At the lower end of the linear range one property becomes important: If the zero-dose (i.e. the dose measured from an unirradiated dosimeter) of a dosimeter is large in comparison to the doses that shall be measured, it becomes increasingly difficult to calculate the correct dose. This is on one hand due to the natural background, which is of course different for different cards. On the other hand, the zero-dose is caused by slight differences in the production process, such as a different temperature. Additionally, dosimeters that were irradiated with high doses have a zero-signal that is still further increased. This is termed the *residual dose*.

3. Basics of Radiation Protection and Dosimetry

3.1. Ionising Radiation

A first classification is possible in ionising and non-ionising radiation, the difference being in the energy necessary to ionise matter. This energy is in the range from 10^{-19} J to 10^{-16} J (0.6 eV - 0.6 keV), depending on the material. Above this threshold one speaks of ionising radiation (Krieger, 2009). Ionising radiation appears in many forms, a division is, e.g., possible in charged and uncharged radiation or whether it is caused by a particle or electromagnetic waves, i.e., photons.

α- or β-particles are prominent examples of charged particle radiation. Neutrons and photons are both uncharged, the first is also counted among particle radiation while photons can be thought of as a class themselves, containing γ- and X-radiation.

Before discussing radiation protection and dosimetry in more detail, some important dose quantities when working with radiation will be recalled.

3.2. Dose Quantities

There are 3 basic classes of dose quantities (Stadtmann, 2001):

- Physical quantities
- Protection quantities
- Operational quantities

They are defined by two commissions, the *International Commission on Radiation Units and Measurements* and the *International Commission on Radiological Protection*, who regularly publish updates or revisions.

3.2.1. Physical Quantities

Important physical quantities are

- kerma and
- the absorbed dose.

They are defined by the International Commission on Radiation Units and Measurements in ICRU Report 85.

Kerma

Kerma stands for *Kinetic Energy Released per unit MAss*. It is defined by

$$K = \frac{dE_{tr}}{dm}, \tag{3.1}$$

where dE_{tr} is the sum of the kinetic energies of all charged particles released by uncharged particles and dm the mass of a volume element. Therefore, it is only defined for uncharged particles (photons or neutrons). The unit of kerma K is Jkg^{-1} and is called Gray (Gy).

Absorbed Dose

The absorbed dose is similar to kerma but is defined by

$$D = \frac{d\bar{\epsilon}}{dm} \tag{3.2}$$

Different to the kerma, $d\bar{\epsilon}$ is now the mean energy absorbed by dm. The unit of the absorbed dose D is Jkg^{-1} and is called Gray (Gy).

3.2.2. Protection Quantities

The important protection quantities are

- the equivalent dose of an organ/tissue and
- the effective dose.

Protection quantities are defined by the International Commission on Radiological Protection in ICRP Publication 103. These quantities cannot be directly measured, therefore the operational quantities are used to estimate the protection quantities.

Equivalent Dose of an Organ/Tissue

The equivalent dose of an organ or tissue takes the different biological effects of the absorbed dose depending on the type of radiation into account. More accurately, the mean absorbed dose $D_{T,R}$ is used, the mean being taken over a tissue (T) and a type of radiation (R). The equivalent dose can then be calculated using the following equation:

$$H_T = \sum_R w_R D_{T,R}, \tag{3.3}$$

where w_R is a weighting factor for different types of radiation (R). The values of w_R for different types of radiation are determined from experimental data and are dimensionless, therefore the unit is the same as for the absorbed dose (Jkg^{-1}) but named Sievert (Sv), to indicate the difference of the definition. The weighting factor w_R for photons is defined as 1.

Effective Dose

Whereas the equivalent dose accounts for different types of radiation through different weighting factors w_R the effective dose goes one step further and also accounts for different types of tissues. This is done by another set of weighting factors w_T for tissues (T):

$$E = \sum_T w_T H_T \tag{3.4}$$

The factors w_T are again determined experimentally. They are normalised, therefore $\sum w_T = 1$ and can be changed to account for improvements in the understanding of the effects of ionising radiation on different types of tissues. The unit is the same as for the equivalent dose (Jkg^{-1}) and also called Sievert (Sv).

3.2.3. Operational Quantities

The operational quantities are used to estimate the protection quantities, which cannot be measured directly. Important operational quantities are

- the ambient dose equivalent,
- the directional dose equivalent and
- the personal dose equivalent.

They are defined by the International Commission on Radiation Units and Measurements in ICRU Report 51.

The dose equivalent appearing in these three quantities should not be confused with the equivalent dose mentioned before. The dose equivalent is defined as

$$H = QD, \tag{3.5}$$

where H is defined at a point in tissue, with D being again the absorbed dose and Q a quality factor at this point. The unit is Jkg^{-1} and again called Sievert (Sv). Although both, the dose equivalent and the equivalent dose, are derived from the absorbed dose they differ as the respective weighting (or quality) factors are calculated differently. Where the weighting factor w_R for the equivalent dose depends only on the type of radiation from the outside, the quality factor Q for the dose equivalent includes secondary radiation from the inside, which is produced in the tissue itself in the course of the absorption process. It is a function of the linear energy transfer in water and can change in a body.

All three types of dose equivalent are defined at a certain point d either inside a sphere (the ICRU sphere for the ambient dose equivalent and the directional dose equivalent) or inside a body (for the personal dose equivalent). For calibration purposes phantoms are used. Depending on the penetration depth of the radiation different depths d are specified:

- 10 mm for strongly penetrating radiation

- 0.07 mm for weakly penetrating radiation (and skin)
- 3 mm for weakly penetrating radiation (and the eye)

The unit is Jkg^{-1} for all three and called Sievert (Sv).

Ambient Dose Equivalent

Written as $H^*(d)$ it is the dose equivalent at a depth d in the ICRU sphere produced by an expanded[1] and aligned[2] radiation field.

Directional Dose Equivalent

The directional dose equivalent $H'(d, \Omega)$ is similar to the ambient dose equivalent but with a specified direction Ω in addition to the depth in the ICRU sphere.

Personal Dose Equivalent

The personal dose equivalent $H_p(d)$ is used in individual monitoring and is the dose equivalent at a specified depth d in a body.

3.3. Radiation Protection

Radiation transports energy, when radiation penetrates matter this energy is absorbed by the matter. From this absorbed energy the various doses described in the last section derive. These quantities are used to describe the effects the ionising radiation has when irradiating matter and in particular living, organic matter. One distinguishes two different types of effects (ICRP Publication 103 and ICRP Publication 118):

- Tissue reactions (formerly deterministic effects)
- Stochastic effects

The difference is that it is possible to give a lower dose threshold for tissue reactions, with no notable effects at lower doses. Stochastic effects have no such threshold, meaning they occur together with tissue reactions at high doses as well as at very low doses.

[1] In an expanded field the fluence and the directional and energy distribution is the same in the whole volume as in an actual field.

[2] An aligned field has the same fluence and energy distribution as an expanded field, but an unidirectional fluence.

3.3.1. Tissue Reactions (Deterministic Effects)

Tissue reactions (formerly deterministic effects), appear after irradiation with doses above a certain threshold. This threshold depends on the material or organ in question. The effects above this threshold are, as suggested by the former name, deterministic and therefore unavoidable whereas no tissue reactions can be noted with lower doses. The threshold for tissue reactions is between 0.1 and 0.5 Gy (Krieger, 2009).

The symptoms of tissue reactions for whole body doses are depicted in table 3.1, ranging from whole body doses of the order of 1 Gy up to several 100 Gy. The time frames or latencies of the symptoms range from weeks (doses of $<$6 Gy) over hours (around 10 Gy) to seconds (1000 Gy). They are caused by directly damaging cellular tissue with subsequent, immediate failure of the biological functions.

At whole body doses below 1 Gy survival is almost certain, at low doses ($<$3 Gy) survival is very likely, if no previous medical conditions exist and no secondary infections occur.

The first symptoms appear at whole body doses $>$1 Gy and usually involve sickness, tiredness, nausea, vomiting and diarrhoea, which set in earlier if the exposed dose is higher. The $LD_{50/30}$[3] is approximately 4.5 Gy with most deaths after the 4th week. The $LD_{100/30}$[4] lies between 6-10 Gy and deaths mostly occur already during the second week, at the latest after the third week. Death is usually preceded by internal haemorrhaging, sepsis and ulceration.

At whole body doses exceeding 10 Gy the symptoms occur increasingly fast, with proteins and the nervous system being destroyed. At doses of 1000 Gy death happens within seconds.

Dose [Gy]	Latency	Symptoms	Survival
0.25-1	-	Small changes in blood count.	Certain
1-2	-	Sickness, tiredness, (vomiting).	Certain
2-3	days-weeks	Sickness, vomiting (days), loss of weight (weeks). Possibility of secondary infections.	Very likely
3-6	hours-weeks	All above. Hair loss, internal haemorrhaging, sepsis (2nd week). Acute radiation syndrome.	50% at 4.5 Gy, $LD_{50/30}$
6-8	hours-days	All above. Internal haemorrhaging (first week).	None.
50-100	hours	Proteins, nervous system destroyed. Severe internal haemorrhaging.	None.
$>$1000	seconds	Nervous system immediately destroyed. Death within seconds.	None.

Table 3.1.: Tissue reactions of a certain whole body dose according to Krieger (2009).

As mentioned before, these are only the direct effects of radiation on tissues. Stochastic effects have no lower threshold, they are assumed to occur always. Whereas doses below

[3]The $LD_{50/30}$ is the dose were 50% of the victims have died within 30 days.
[4]The $LD_{100/30}$ is the dose were 100% of the victims have died within 30 days.

3 Gy usually are not lethal, the long-term effects can be.

3.3.2. Stochastic Effects

Stochastic effects are not caused by direct damage of cellular tissue. Instead the genetic code is damaged or changed which results in malign growth causing tumors, leukemia or cancer. There is no minimum or lower threshold for stochastic effects as there is for tissue reactions, which means that also for very small doses there is (supposed to be) a certain chance of radiation damage, albeit a very little one. This model is called *linear no-threshold* (LNT) (Krieger, 2009) and allows the simple summation of small doses, which would not be possible in a non-linear case.

To give certain data concerning the effects of stochastic radiation damage is difficult. An important source are the surviving victims of the two atomic bombings of Hiroshima and Nagasaki. They have been monitored to be able to estimate long term effects of radiation. The risk to acquire lethal cancer is 5 %/Sv of effective dose at low dose rates and 10 %/Sv of effective dose at high dose rates.

As there is no minimal dose at which stochastic radiation effects start to occur, the lower limit at which radiation can be detected should be kept as low as possible, because small doses acquired over longer durations add up and can also have harmful effects. A fundamental rule for radiation protection is the so called ALARA principle, meaning *As Low As Reasonably Achievable*. In accordance with this principle there are guidelines that control the amount of radiation human beings are allowed to be exposed to. In Austria the regulations are as follows: Persons who are professionally exposed to radiation are classified according to two categories:

- **Category A:** Professionally to radiation exposed persons who are expected to receive an effective dose of *more than* 6 mSv, a dose equivalent of 45 mSv for the eye lens and of 150 mSv for skin, hands, arms, feet and ankles in 12 consecutive months.
- **Category B:** Professionally to radiation exposed persons not contained in category A.

Additionally, for professionally to radiation exposed persons the effective dose must not exceed 20 mSv in 12 consecutive months. Under certain conditions it is possible for persons in category A to receive an effective dose of 50 mSv in single years, as long as the accumulated effective dose over 60 consecutive months (5 years) does not exceed 100 mSv (i.e. overall the annual limit of 20 mSv still holds).

These limits are defined in the Council Directive 2013/59/EURATOM of the European Union and in the BGBl 2012/191 (Bundesministerium für Land- und Forstwirtschaft, Umwelt und Wasserwirtschaft, Österreich, 2012).

Simplified, persons in category B may receive up to 6 mSv per year and persons in category A more than 6 mSv but less than 20 mSv. For comparison, the worldwide averaged background from natural radiation sources is 2.4 mSv per year (UNSCEAR 2008 Report). Here, 1.26 mSv are caused by the inhalation of radioactive radon, which emits α-radiation. As mentioned in section 2.4, the dosimeter used during this study can only be used for the

detection of beta and gamma radiation. The natural background, excluding the dose from radon, is 1.14 mSv per year, which is about 95 μSv per month.

To keep these limits it is necessary to monitor whenever radiation related work is done. It is also necessary to be able to measure even low doses: the 6 mSv per year limit for category B is equal to 500 μSv per month. Compared to the natural background of about 95 μSv per month this is larger only by a factor $\approx$5. It should therefore be possible to measure doses at least of the same order as the natural background.

3.4. Radiation Protection Dosimetry

Whenever a person is working with radiation it is necessary to monitor and record the amount of radiation received. As described in the previous sections about the effects of radiation there are tissue reactions (section 3.3.1) occurring at high doses of more than 0.25 Gy and stochastic effects (section 3.3.2) already occurring at much lower doses. Therefore, it must be possible to know immediately if a high dose has been received in short times as well as to know the total accumulated amount over longer times. The first one is done by active dosimetry and the latter mainly by routine/passive dosimetry.

Active or direct-read dosimeters are dosimeters where, as the name suggests, the dose is displayed immediately. Usually it is possible to activate an acoustic alarm function that gives a warning when a certain dose threshold is exceeded. These dosimeters are treated in the International Standard IEC 61526 and further described in the next section (3.4.1).

Passive dosimeters do not allow the direct display of doses. They are usually worn for a certain period, e.g., one month and record the dose during that time. By a readout the dose for the month is determined. The second important application is for environmental monitoring. Passive dosimeters for personal and for environmental monitoring are treated in the International Standard IEC 62387-1 and further described in section 3.4.2.

3.4.1. Active dosimeters

Active dosimeters allow a direct readout of the dose. Usually they use electronic methods to detect ionising radiation.

The basic process is that voltage is applied to a capacitor and incoming radiation ionises the particles between the electrodes. The ions and electrons are then separated according to their charge and an electric current flows until all charged particles are absorbed.

As the dose is directly displayed or at least recorded it is possible to immediately alert the wearer of a sudden dose rate increase or an exceeded amount of dose. This is especially important when working with radioactive sources.

3.4.2. Passive Dosimeters

As mentioned, in contrast to active dosimeters, passive dosimeters do not allow for a direct display of the dose. They need to be actively read out to determine the accumulated dose over a certain amount of time. Passive dosimeters are usually worn routinely, whereas active

dosimeters are sometimes worn additionally when a direct display of the dose is needed. In routine dosimetry, each person has a personal dosimeter, which is worn (for example) for one month and then returned to the dosimetry service, where the dose is read out and reported back.

The second application is for environmental dosimetry, for which the dosimeter is not worn but placed at a fixed location for a certain amount of time.

Originally, mainly film badge dosimeters were used for passive dosimetry, which recorded the amount and possibly the direction of ionising radiation through the blackening of photographic film. Recently, film badge dosimeters are more and more replaced by more modern devices, e.g., by thermoluminescence dosimeters. An important improvement is the wide dose range these dosimeters can be used with, ranging from doses of a few μSv up to several 100 Sv. However, to use these dosimeters a calibration is necessary as the emitted light cannot directly be related to a dose the dosimeter was irradiated with.

Thermoluminescence dosimeters and difficulties arising with their usage shall be described in more detail in the following.

3.5. Thermoluminescence Dosimetry

As mentioned before, thermoluminescence dosimeters are routinely used in personal dosimetry. They make use of the ability of thermoluminescence crystals to store the energy of ionising radiation and release this energy again as light when the crystal is heated. The materials used for dosimetry are described in the section about thermoluminescent materials (section 2.4). Thermoluminescence (TL) dosimeters are treated by the International Standard IEC 61066.

3.5.1. Methods of Dose Calculation

To calculate a dose from an irradiated TL dosimeter the dosimeter needs to be read out. This happens by heating the crystal, which releases the stored electrons and emits light (see section 2.2 and figure 2.1). The light is recorded over the whole duration of the heating process which yields the glow curve. To calculate a dose from the glow curve several methods are possible, usually summarised under the term *computerised glow curve analysis* (CGCA) (Horowitz and Moscovitch, 2012). The first method is to calculate the dose by measuring the area below the glow curve, which is the total amount of emitted thermoluminescence. Another possibility would be to measure the height of the dosimetric peak and with it calculate the corresponding dose. The third, more complex method, tries to deconvolute the glow curve into a series of single peaks and thus receive information about the amount of energy stored at the different traps. This *computerised glow curve deconvolution* (CGCD) (Horowitz and Yossian, 1995) yields a lot of information about the glow curve, most importantly the peak parameters. It is, however, more complex and time consuming.

The method used in the dosimetry service at Seibersdorf measures the area below the whole glow curve. Not relevant peaks with too high fading are eliminated by annealing the dosimeter at a lower temperature before the readout.

4. Experimental Facilities and Procedures

4.1. The TLD-100 System

The TLD-100 system is a thermoluminescence dosimeter used for personal dosimetry, for example in medicine or industry. The dosimeters are usually worn for one month and then sent to a readout laboratory. The radiation sensitive part is manufactured as chips with a size of 3.2x3.2 mm^2 and a thickness of 0.38 mm. These are encased in Teflon within two aluminium sheets. Depending on the application between 2 and 4 chips (or elements) are included in one dosimeter. The aluminium card is normally sealed and worn in a card holder. Figure 4.1 depicts a TLD-100 card with the card holder. This card has two elements, one of which is shielded by an aluminium disc. As mentioned earlier (see section 2.4) it is possible to manufacture dosimeters that can detect a neutron dose. This is done by adding two more elements with a different lithium isotope composition. The different isotope is neutron sensitive and stores energy from neutrons together with energy from beta and gamma radiation. The difference between the neutron sensitive and the non-sensitive elements yields the neutron dose.

Seibersdorf is one of the readout laboratories in Austria and does the analysis of most of the TLDs used in the country. As mentioned, it is not possible to directly get the dose that a TLD is exposed to from the light detected while heating it. Therefore, careful calibration needs to be done in order for the data to be usable. Seibersdorf makes use of the irradiation facilities on the area, the Seibersdorf Dosimetry Laboratory (DEL), where cards are irradiated in a controlled environment with known doses. These are then read out together with the routine cards received from customers, which in turn allows for the actual doses of the routine cards to be calculated. The actual calibration process is a bit more complicated though and includes another step, where the calibration cards themselves are calibrated. This shall be described in more detail in the following section.

Figure 4.1.: On the left side a TLD-100 card is shown containing two chips of LiF:Mg,Ti at card positions 2 and 3 (red circles). This card is then sealed and provided to the customer (in the centre). On the right side the card is shown as placed in the card holder. One of the two elements is shielded with a thin aluminium disc (yellow circle). This allows to apply different weights for hard and soft radiation.

4.1.1. Readout

The readout of all cards is done using a Harshaw TLD Reader 8800 (further described in section 4.3). The readout of one card yields 2-4 values, one for each element (or crystal). Each card has a certain individual correction factor for each element (k_i, where i is the position of the element) which are determined by a calibration process before the card is used the first time and then thereafter on a regular basis.

Each time a set of 200 cards is readout on a machine, a second calibration factor fe_i comes into play, which is the same for all cards in the corresponding set and is the calibration factor of the machine. The factor fe_i is determined with the help of calibration cards, which are always irradiated with the same dose. They are always read out together with the routine cards and the quotient of the mean of their irradiated and measured dose gives the calibration factor fe_i.

The factor $TL_{kalib,i}$ is the measured dose of each calibration card, k_i is the individual correction factor of the elements and m_i the uncorrected measured value. The value LW is the assumed zero-dose (*Leerwert*), which is 25 μGy for all dosimeters. A card-dependent value for LW, the residual dose, will be investigated in section 5.4.

$$TL_{kalib,i} = (k_i m_i - LW) \tag{4.1}$$

The mean of all measured doses $TL_{kalib,i}$ from the calibration cards is calculated (M_i) and the irradiated calibration dose (5 mGy), K_a, is divided by this value. This then gives equation 4.1 for the fe_i-values. The irradiation of the calibration cards is done at the Dosimetry Laboratory (DEL), further described in section 4.2.

$$fe_i = \frac{K_a}{M_i} \tag{4.2}$$

Once the calibration factor fe_i is known, the dose of the element is calculated by equation 4.3.

$$TL_i = fe_i \cdot (k_i m_i - LW) \tag{4.3}$$

Therefore, correction factors are applied for individual crystals as well as for the whole batch of crystals read out together.

In the TLD-100 system only the elements 2 and 3 are used, therefore we get the values TL_2 and TL_3. Finally, different weighting is applied for hard and soft radiation, which combines the two values TL_2 and TL_3 to one dose value for the dosimeter.

4.1.2. k_i-values

The k_i values need to be calculated beforehand by a separate calibration of the cards. This is done for routine cards roughly every 5 years. This calibration process is different from the above mentioned calculation of the fe-factors (and thereby the calibration of the reader) in that it makes use of the built-in source of the Harshaw TLD Reader 8800. The routine cards are read out together with several reference cards, where each card is also irradiated with the

same dose. As the k_i-values of the reference cards are known, the irradiated dose is known and for each crystal an individual factor can be calculated.

The k_i-values of the reference cards are calculated by another set of cards irradiated at the DEL.

4.2. Dosimetry Laboratory (DEL)

In this section the facilities where the irradiations were carried out will be described. All of these facilities are situated at the Dosimetry Laboratory (DEL) in Seibersdorf. The DEL maintains primary and secondary standards in cooperation with the *Bundesamt für Eich- und Vermessungswesen* (BEV). It is a dosimetry laboratory certified as an *Accredited Body for Calibration* (Akkreditierung Austria, 2015a) as well as an *Accredited Body for Testing and Inspection* (Akkreditierung Austria, 2015b).

It consists of the following facilities used for irradiations:

- One panoramic irradiation facility (PIF)

and two collimated beam irradiation units, the

- Reference irradiation facility (RIF) and the
- Teletherapy unit (TU).

Apart from these nuclide sources five X-ray tubes are available, which have not been used for this study.

4.2.1. Panoramic Irradiation Facility (PIF)

The panoramic irradiation facility (figure 4.2) allows the irradiation of a large number of cards at once. For this purpose the cards are arranged in a semicircle around a vertical pipe into which the radioactive source is injected and removed by air pressure.

The amount of dose that the TLDs are irradiated with is determined on the one hand by the selection of one of four sources and on the other hand by the duration of the irradiation. The four sources are Cs-137 sources.

The half-life of Cs-137 is known and the activity of all sources is certified by the BEV. Therefore, the actual activity and dose rate can easily be calculated for the date of the irradiation. The sources are stored in a safe outside the irradiation chamber in a rotating cylinder. After the selection of a source and the start of the irradiation process the source is injected into the irradiation chamber with pressurised air. After the selected time has passed, the source is removed back into the safe again using pressurised air. The injection and removal processes take approximately 0.8 s, which is considered in the calculations. To keep the uncertainty for the irradiated dose low, durations of at least 100 s are recommended where possible. Irradiation times can be selected with one-tenth of a second accuracy.

The panoramic irradiation facility is calibrated for a fixed distance. A PMMA stand allows the placement of up to 116 TLD-100 cards in two rows of 58 cards in a semicircle around the source.

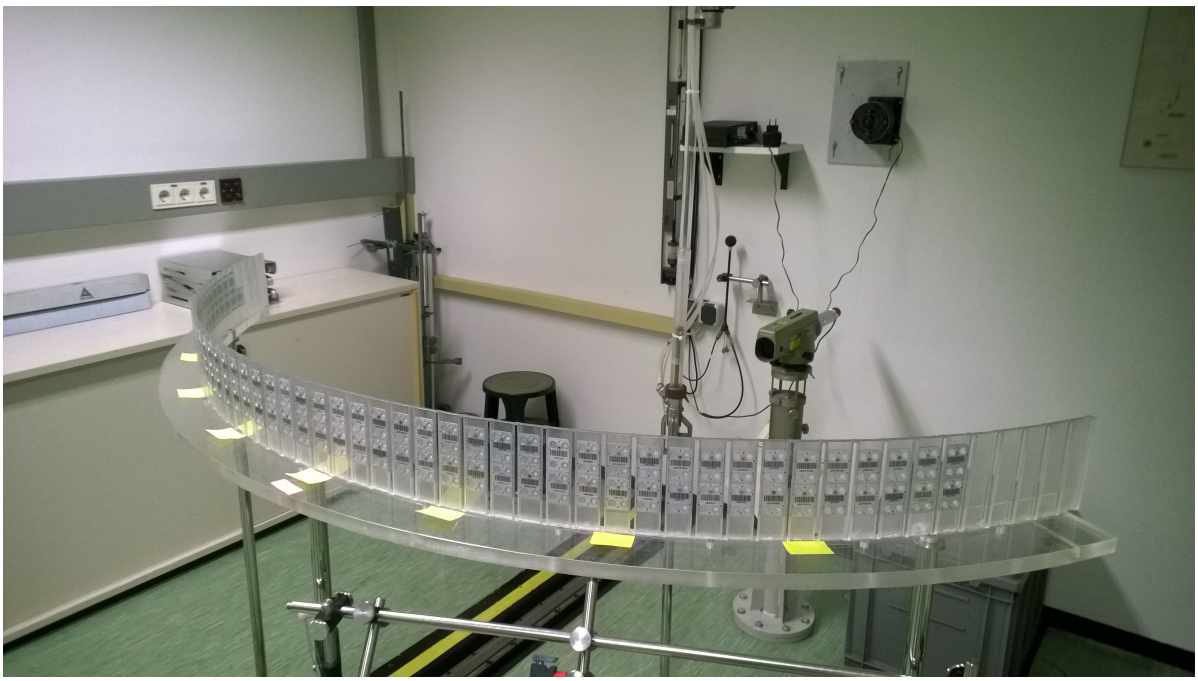

Figure 4.2.: Panoramic irradiation facility. The cards are arrayed in a semicircle and the source enters the tube from the top.

4.2.2. Reference Irradiation Facility (RIF)

The reference irradiation facility (figure 4.3) is a collimated beam unit, where the source is positioned behind a shutter that is removed to start the irradiation. It provides 6 different sources made of two different elements (Co-60 and Cs-137) which are moved from a safe into position automatically when selected. Only then the shutter opens and the irradiation begins. In contrast to the panoramic irradiation facility the distance to the source can be varied.

The variable distance to the source gives a good control over desired dose rates and allows very low dose rates by positioning the cards at high distances. The distance may be varied between 500 mm and 18000 mm, depending on the installation. The distance is measured by the movable carriage and has to be set and calibrated once manually at the beginning of the irradiations as the position of the reference point on the carriage is dependent on the set-up.

4.2.3. Teletherapy Unit (TU)

The teletherapy unit (figure 4.4) is also a collimated beam unit, where the sources are placed behind a shutter. It has only one source made of Co-60. The dose rate is therefore only dependent on the distance to the source. Additionally, the aperture can be varied between two set-ups: One with a 10x10 cm field (measured in a distance of 1 m to the source) and one with a 20x20 cm field. For the conducted irradiations the second aperture was selected in order to be able to irradiate more cards at the same time. To ensure a homogeneous

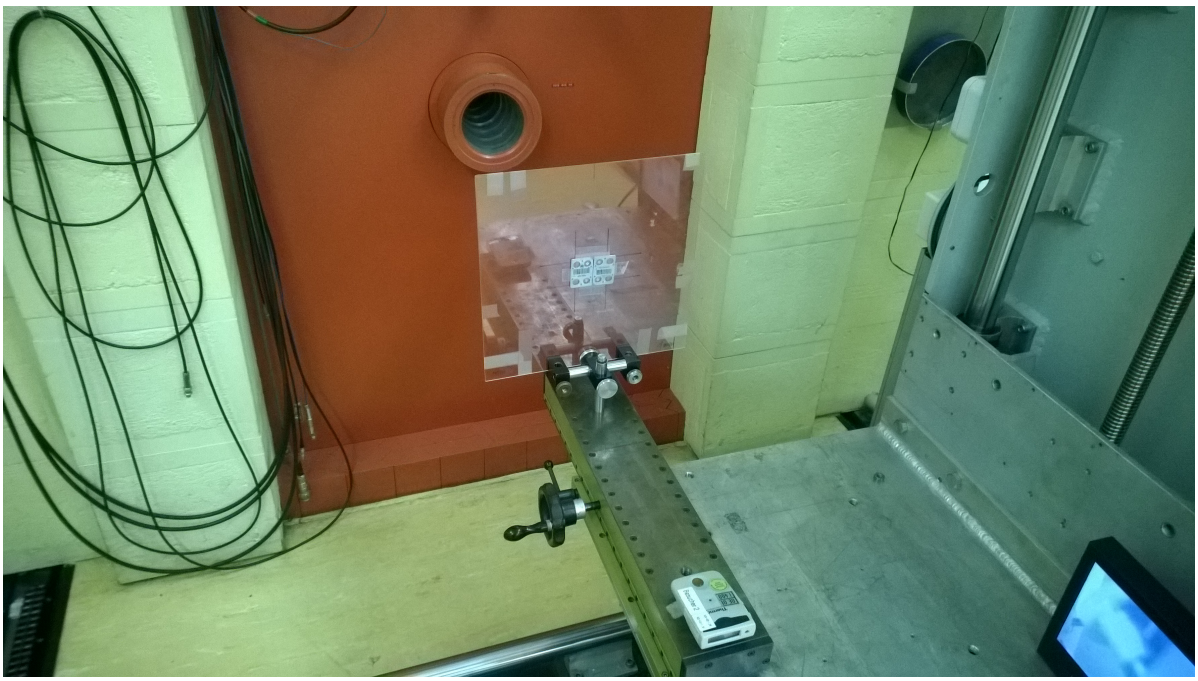

Figure 4.3.: Reference irradiation facility. The cards are positioned in the beam. The shutter is at the end of a shaft to increase the collimation. The cards are fixed on a carriage that can be moved up to 18 m away from the source.

irradiation the cards were only placed in an area half the size of the field. For irradiations of low doses a lead absorber can be added into the path of the beam which significantly lowers the dose rate.

The distance may be varied between 600 mm and 5000 mm. As with the reference irradiation facility, the distance is measured by the movable cart and has to be set manually at the beginning of the irradiation experiment.

4.3. Harshaw TLD Reader 8800

The Harshaw TLD Reader 8800 is a reader produced by Thermo Scientific which is used for the routine dosimetry procedure at Seibersdorf. The cards that were irradiated in the course of this study were also read out using one of the four available machines.

The reader can be loaded with approximately 1400 cards in 7 cartridges of 200 cards each. During the readout procedure a card is removed from the cartridge and the bar-code (see figure 4.1 on the left hand side) is read. The TLD crystals encased in the card are then heated up by 4 beams of hot nitrogen in a predetermined temperature profile (TTP), while a photomultiplier records the emitted light. The temperature profile used in the routine measurements heats the crystals to 280 °C and takes a total time of 13.3 s. The temperature profile will be discussed in more detail later on in section 5.1.1. In certain cases the card is read out repeatedly. After the readout process is done the card is passed to a second set of

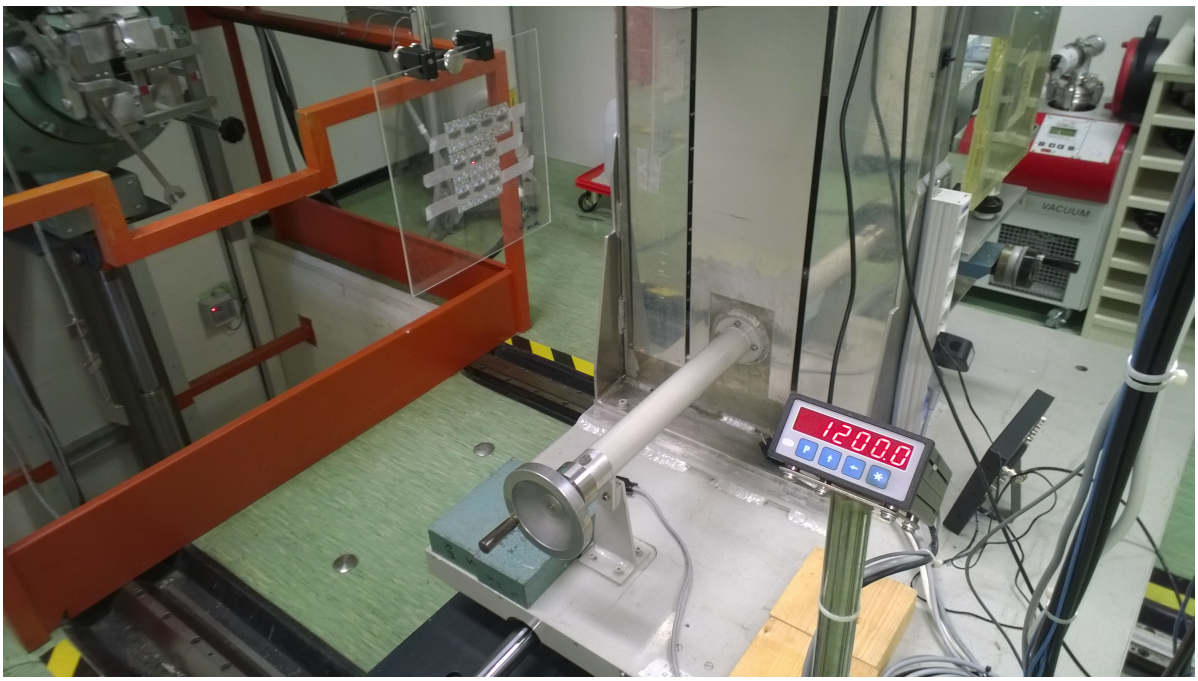

Figure 4.4.: Teletherapy unit.

cartridges where the finished cards are collected.

4.4. Irradiations

As described in section 4.2, Seibersdorf provides several facilities to carry out controlled irradiations. This allows a comparison of the measured data from the readout procedure with the actual irradiated dose and to look specifically at certain ranges of doses. In the course of this study a total of 8 irradiation experiments were carried out at the Seibersdorf Dosimetry Laboratory (DEL).

Table 4.1 gives an overview of the dose ranges and the number of irradiated cards for each irradiation procedure. All doses are in air kerma (K_a). The doses cover a range of seven orders of magnitude, from 30 μGy to 190 Gy, or $3{\cdot}10^{-5}$ Gy to $1.9{\cdot}10^{2}$ Gy.

The results of the irradiations are presented in chapter 5: Irradiations No. 1 and No. 2 are used for the wide dose range linearity measurement (section 5.2) and the high dose supralinearity investigation (section 5.3). In the course of this irradiation the cards used for the glow curves shown in section 5.1.2 were also irradiated. Irradiations No. 3 to No. 5 are used for the investigation of possible methods of background correction in section 5.4. With irradiation No. 6 it was tried to increase the upper limit of the supralinearity investigation. This, however, proved to be above the range of detection of the reader. Irradiations No. 7 and No. 8 are used to improve the conversion from cobalt to caesium dose.

All irradiations were designed in such a way that a reference point of a 5 mGy irradiation with Cs-137 was always included. This was done to replace the calibration cards that would

Irradiation No.	Dose range, K_a	Cards	Date	Facility
1	30 μGy - 10000 μGy	399	22.4.2014	PIF
2	5 mGy - 10000 mGy	58	30.4.2014	TU, RF
3	200 μGy - 20000 μGy	457	20.5.2014	PIF
4	200 μGy - 20000 μGy	457	12.6.2014	PIF
5	200 μGy - 20000 μGy	457	30.6.2014	PIF
6	17 Gy - 190 Gy	36	4.9.2014	TU
7	5 mGy - 10 mGy	15	2.12.2014	PIF, TU
8	5 mGy - 10 mGy	11	3.12.2014	RF

Table 4.1.: Overview of the irradiations carried out at the DEL.

otherwise be needed. The dose of 5 mGy is therefore the point where the irradiated dose exactly equals the measured dose. The irradiations were done using both cobalt and caesium sources, which have a different energy dependence. Therefore, to enable an evaluation of the linearity across a wide dose range, all irradiated doses are given as caesium doses. The cobalt doses were converted to caesium doses by measuring the conversion factor.

The cards that were used during this thesis were provided by the Seibersdorf Labor GmbH. All cards are identified by a serial number and all executed irradiations were recorded for all cards. All in all, 457 different cards (TLD-100) were used. Among these were 399 routine cards, which were used only for low to medium dose irradiations to avoid card damage. The rest, 58 cards, were previously sorted out from the routine dosimetry programme due to a slightly increased residual dose. These were used for high dose irradiations.

Type	Number of cards
Defect	58
Routine	399
All	457

Table 4.2.: The different cards used for this study. The actual numbers of cards used for the irradiations is usually lower, as each time 10-20 % were not irradiated and instead used to calculate the transport dose from the natural background.

4.5. Measurements

The measurements or readouts of the cards were done on the Harshaw TLD Reader 8800 described in section 4.3. For all readouts the standard temperature profile with a heating rate of 30 Ks^{-1}, a start temperature of 50 °C, a maximum temperature of 280 °C and a duration of 13.3 s was used (see figure 5.2). The exceptions were the readouts used to acquire the glow curves in section 5.1.2, where the maximum temperature was set to lower values and the duration of the readout was increased to up to 53.3 s.

The standard readout procedure records a reread only when the previous read exceeds a dose of 150 μGy. By lowering this threshold a series of rereads can be measured. The number of rereads of each readout procedure was varied between and 4 and 9. The nature of the cards necessitates that all the needed information is acquired in one run, because any information not recorded is erased and destroyed in the very same process. Reading out at a later time is problematic because an unknown dose from the natural background is stored during this time. Therefore, a compromise has to be found between recording a large number of rereads while at the same time keeping the duration of the readout of all cards as short as possible.

Usually, whenever a card is read out, an automatic routine is run that calculates the dose by applying the k_i-factors to the two elements of the dosimeter, the fe-factor to the whole readout procedure and weights to the shielded and unshielded elements of the card. Thus, one single personal dose is received from one card. For this thesis, however, all cards were irradiated with both elements unshielded and without using a water phantom. As the irradiations were calculated using air kerma, the result is also in air kerma. The two elements of each card were therefore treated separately as independent detectors, yielding a *crystal dose* in air kerma (with the unit Gy) rather than a personal dose (with the unit Sv). This does not change the applicability to real dosimetry measurements, as the response of the single crystals is independent of the quantity.

4.6. Data from Routine Dosimetry

Apart from the irradiations carried out, anonymous data from the Seibersdorf routine dosimetry programme was used. The readouts of the calibration cards of the last 10 years are used for the long term investigation of the influence of frequently applied medium range doses (see section 5.5).

5. Results and Discussion

5.1. Glow Curve Analysis

5.1.1. Simulation of Glow Curves

The simulation of glow curves was done using the first order model (Randall and Wilkins, 1945a) described in section 2.3.1. The intensity $I(T)$ depending on the temperature T is given as calculated by equation 2.3.

The intensity therefore depends on the heating rate R, with the simplest case being a constant heating rate (see equation 2.3). Figures 2.2 and 2.3 were calculated using a constant heating rate of 30 Ks^{-1}. Figure 5.1 shows what happens to a single peak when the heating rate is decreased: the maximum of the peak shifts to higher temperatures while at the same time decreasing in height. To compare different glow curves, the heating rate should be the same for each measurement as well as constant during the measurement.

Up to now, the glow curves were calculated and plotted with the intensity I depending on the temperature T. The glow curves shown in this section use the intensity $I(t)$ which depends on time. The time dependence of the glow curve is realised by a time dependence of the temperature, which is given by the so-called heating profile (see the section 3.5.1 on the TLD-100 system in use). This allows a more direct control of the heating process.

The heating profile T(t) (or time-temperature profile, TTP) used has an area of linear increase from 50 °C to 280 °C with a heating rate of 30 Ks^{-1} followed by an area of constant temperature. The whole process has a duration of 13.3 s and is shown in figure 5.2 as the dashed blue line.

As mentioned before, the heating is done with a hot nitrogen stream. This has advantages over former methods of heating that used ohmic resistance to heat the TL material in the dosimeter, as it works contactless, the reaction time is fast and the temperature easy to control (Moscovitch et al., 1990).

Nevertheless, the TL chip will not heat instantaneously, instead there will be a certain lag due to heat flow. This has been investigated by Stadtmann et al. (2002) where the following differential equation (5.1) was used to model the real temperature profile.

$$\frac{dT_{LiF}(t)}{dt} = A[T_{gas}(t) - T_{LiF}(t)] + B[T^4_{reader} - T^4_{LiF}(t)] \tag{5.1}$$

Here, $T_{LiF}(t)$ is the temperature of the TL chip and the real temperature profile (the red line in figure 5.2), $T_{gas}(t)$ is the temperature of the nitrogen stream and the selected TTP (the dashed blue line in figure 5.2) and T_{reader} is temperature of the surroundings (approximately room temperature). The constants A and B have been determined to be A

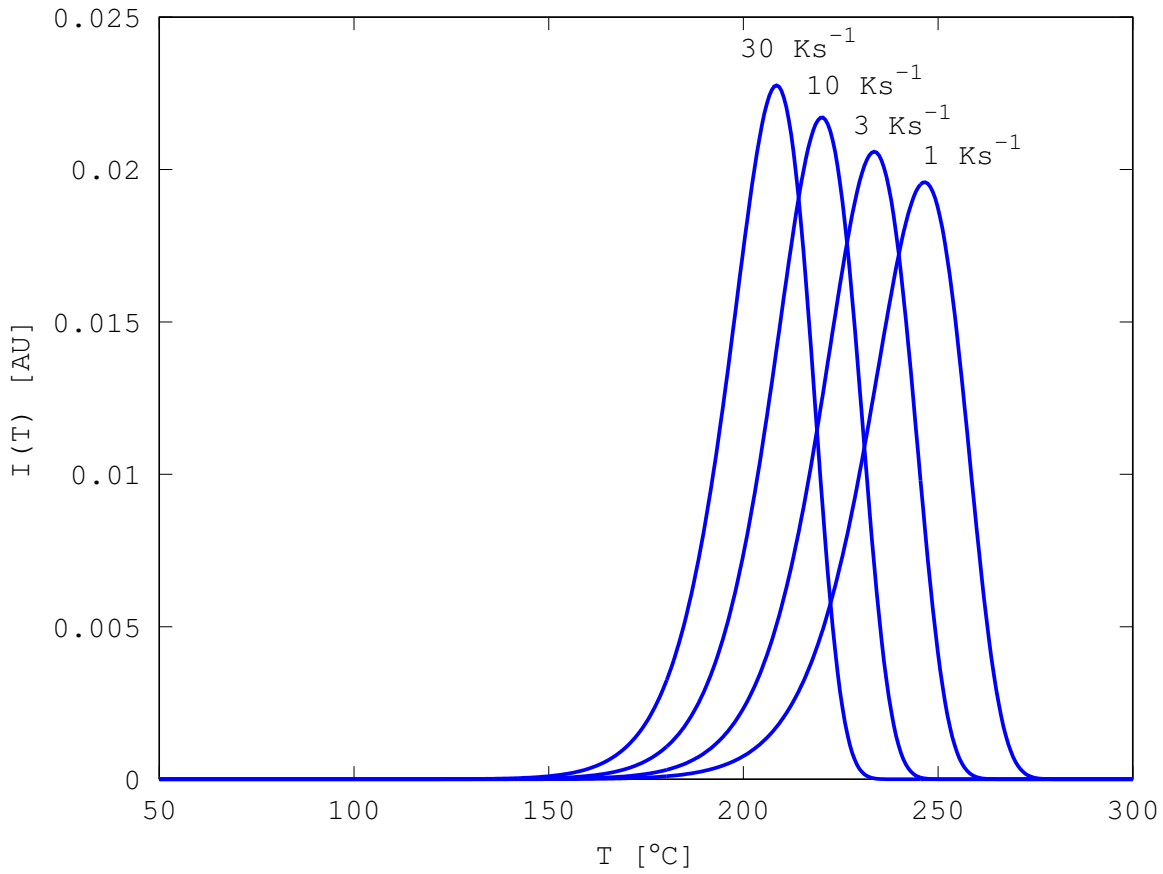

Figure 5.1.: Effects of different heating rates on peak height and the position of the peak maximum. Decreasing the heating rate shifts the peaks to higher temperatures. The heating rates of the peaks are (from left to right) 30, 10, 3 and 1 Ks^{-1}.

$= 0.5\,s^{-1}$ and $B = 2.7{\cdot}10^{-11}\,K^{-3}s^{-1}$ (Stadtmann et al., 2002). The parameters have also been found to be dependent on the mass of the chip (Stadtmann et al., 2006).

The increase of the temperature of the chip depends on the difference of the temperature of the nitrogen gas and the chip (the term after constant A) and on the heat radiated to the surroundings with temperature T_{reader} according to the Stefan-Boltzmann law of Black body radiation. With the introduction of this differential equation, the heating rate is of course not constant anymore.

The differential equation was solved using the free software package GNU Octave. Figure 5.2 shows the acquired solution for the temperature of the TL chip $T_{LiF}(t)$ (red line) compared to the gas temperature (dashed blue line).

The actual temperature of the chip lags behind the temperature of the TTP and never reaches the maximum temperature. An increase in the duration of heating process leads to an equilibrium with the chip temperature being slightly lower than the gas temperature (figure 5.3).

This leads to a shift to higher temperatures of the whole glow curve, as temperatures are

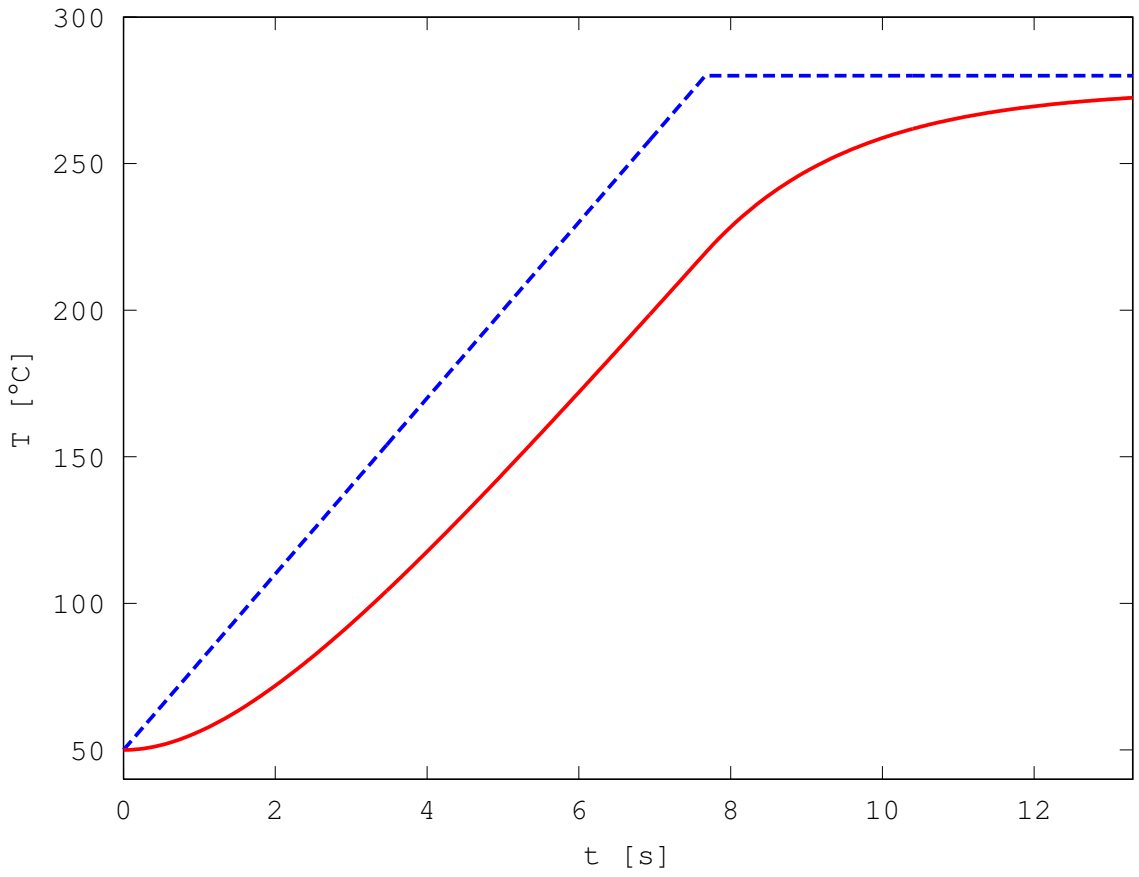

Figure 5.2.: Gas temperature and selected TTP for the readout of the TLD-100 (blue dashed) and the actual temperature profile acquired by solving the differential equation 5.1 (red). The temperature reached at the end of the glow curve is approximately 272 °C, which is 8 °C less than the gas temperature of 280 °C.

reached later than they would if the TTP was an ideal one. This can be seen when the intensity is calculated (again using the first order model) with the real temperature profile. The results are shown in figures 5.4 and 5.5, which apply the ideal TTP and the real TTP, respectively.

It should be noted that the electron populations of the traps, which corresponds to the peak area, are set to arbitrary values to qualitatively construct a resemblance to real glow curve. Usually, dose calculations work the other way around: the trap populations are calculated by a deconvolution of a glow curve.

Notable in figure 5.4 is the sudden drop to zero of the intensity once the maximum temperature is reached. This is caused by a dependence of the intensity (equation 2.3) on the heating rate, which abruptly drops to zero at this point and also reduces the factor $e^{-\frac{s}{R}}$ to zero and thus at the same time the intensity. This behaviour is neither seen in real glow curves nor in the glow curve simulated with the real temperature profile (figure 5.5), because the heating rate only gradually decreases as the maximum temperature is

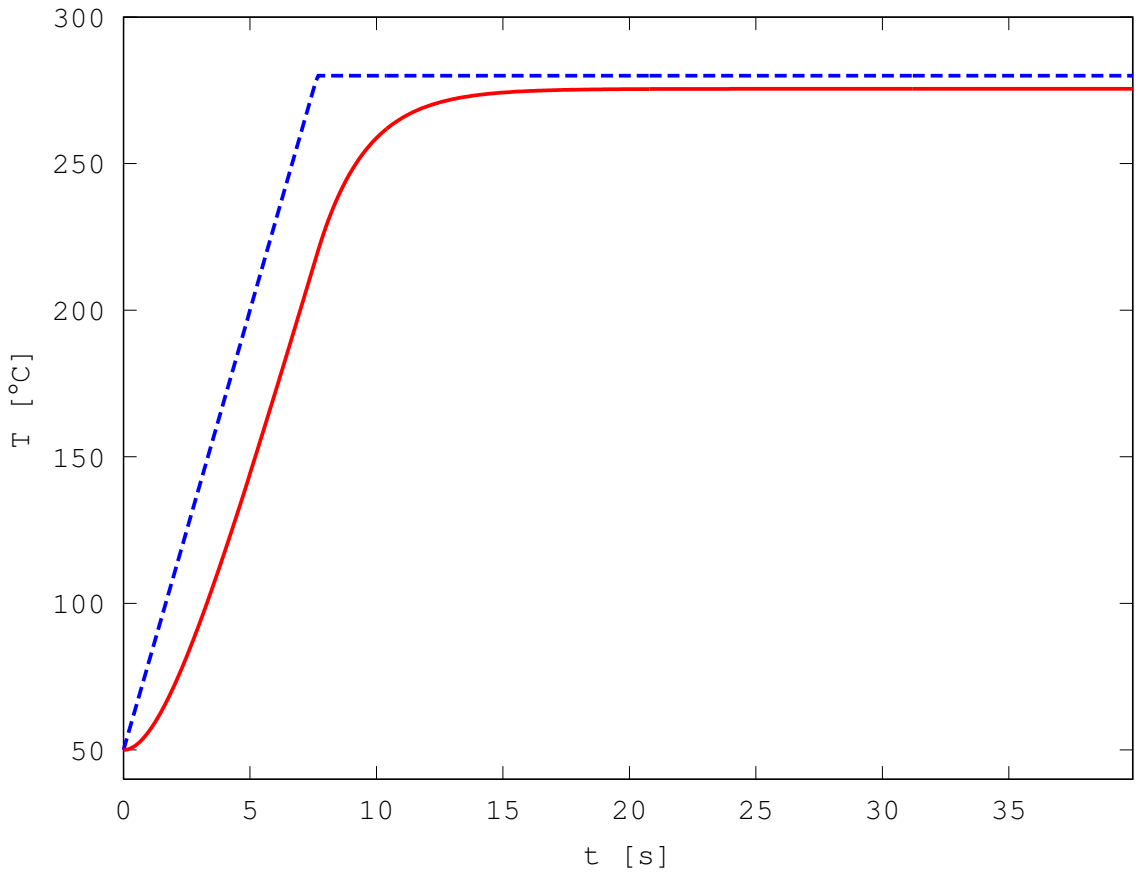

Figure 5.3.: TTP with increased length (blue dashed) and the actual temperature profile acquired by solving the differential equation 5.1. An equilibrium is reached at the end of the profile with a chip temperature of approximately 276 °C, which is 4 °C lower than than the gas temperature of 280 °C.

approached. Temperatures are reached later or not at all and as the actual heating rate becomes smaller, the intensity decays to zero.

This gradual decrease is also the cause of the shift to higher temperatures easily seen in a comparison of the two glow curves. The most prominent effect though is that where before application of the real temperature profile the glow curve exhibited two prominent peaks there only exists one peak when the real temperature profile is used. In figure 5.4 all peaks up to the 5^{th} and 6^{th} peak are clearly visible and peak 7 is cut off. In figure 5.5 only the peaks up to peak 5 are visible. Peak 6 is reduced to a small background at the end of the glow curve and peak 7 is nearly invisible.

Apparently only part of the electrons stored at these traps are released, as is suggested by the small peak 6 in figure 5.5, which only starts to rise as the end of the readout procedure is reached. This means that electrons remain in this trap and these would then be released the next time the dosimeter is heated, causing a residual dose. Peak 7 is even less visible, therefore even more electrons remain in the corresponding trap.

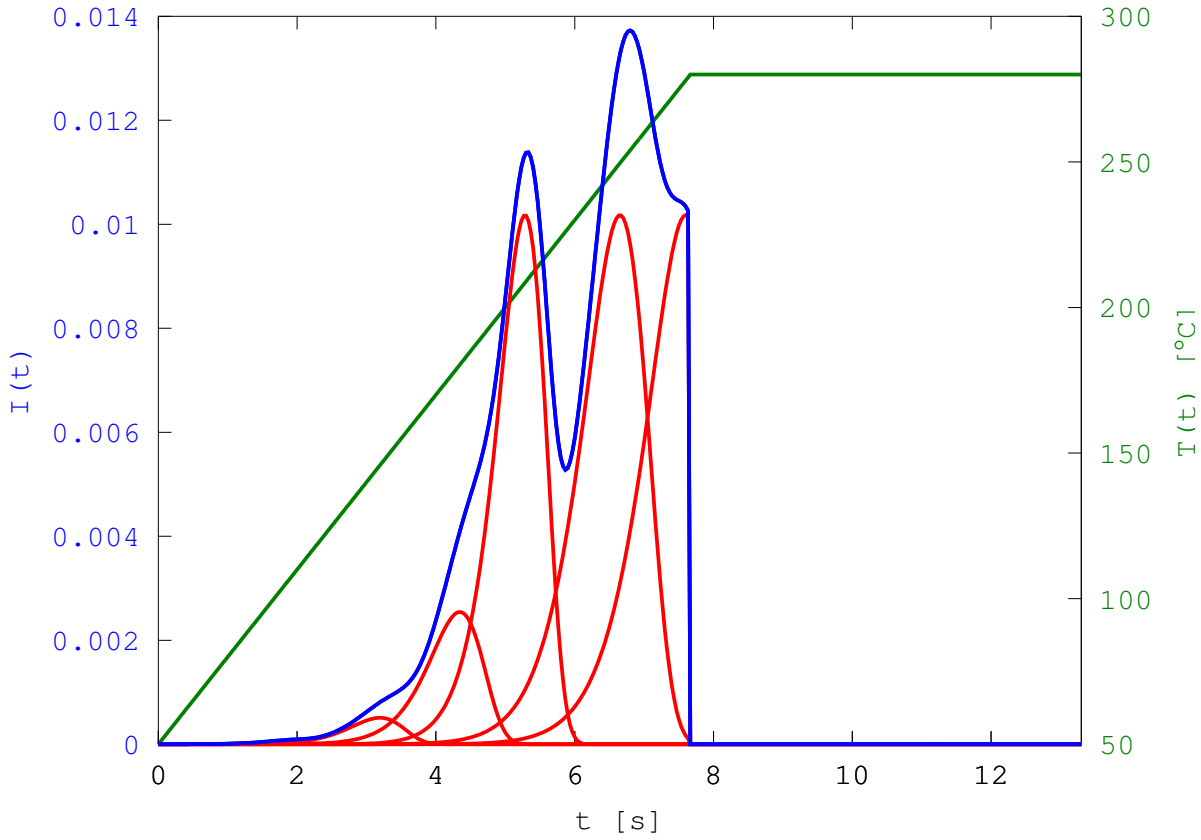

Figure 5.4.: Glow curve simulated with the first order model by Randall and Wilkins (1945a) using the ideal TTP and peaks 2 - 7 from table 2.5. The sudden cutoff after approximately 8 s is caused, in this simulation, by the heating rate R dropping to zero after the maximum temperature is reached. This is because the first order model needs a greater than zero heating rate.

There are still possibilities to release this electrons though:

- A lengthened anneal at high temperatures would increase the chance of electrons being released even from high traps. This has been tried and will be discussed in the next section, concerning measured glow curves 5.1.2.
- It is possible to release electrons from deep traps by irradiating a sample with ultraviolet light. If the irradiation happens at room temperature, the released electrons are retrapped at lower energy traps. By doing a second readout these electrons can also be released. This technique is known as *Ultraviolet light bleaching* and, apart from erasing deep traps, can be used to re-estimate the dose (Mason et al., 1977).

It is not always possible to increase the readout length, especially in a routine readout procedure with thousands of dosimeters. Ultraviolet light bleaching is also time consuming, therefore the approach in this thesis is to find a different way to correct the residual dose.

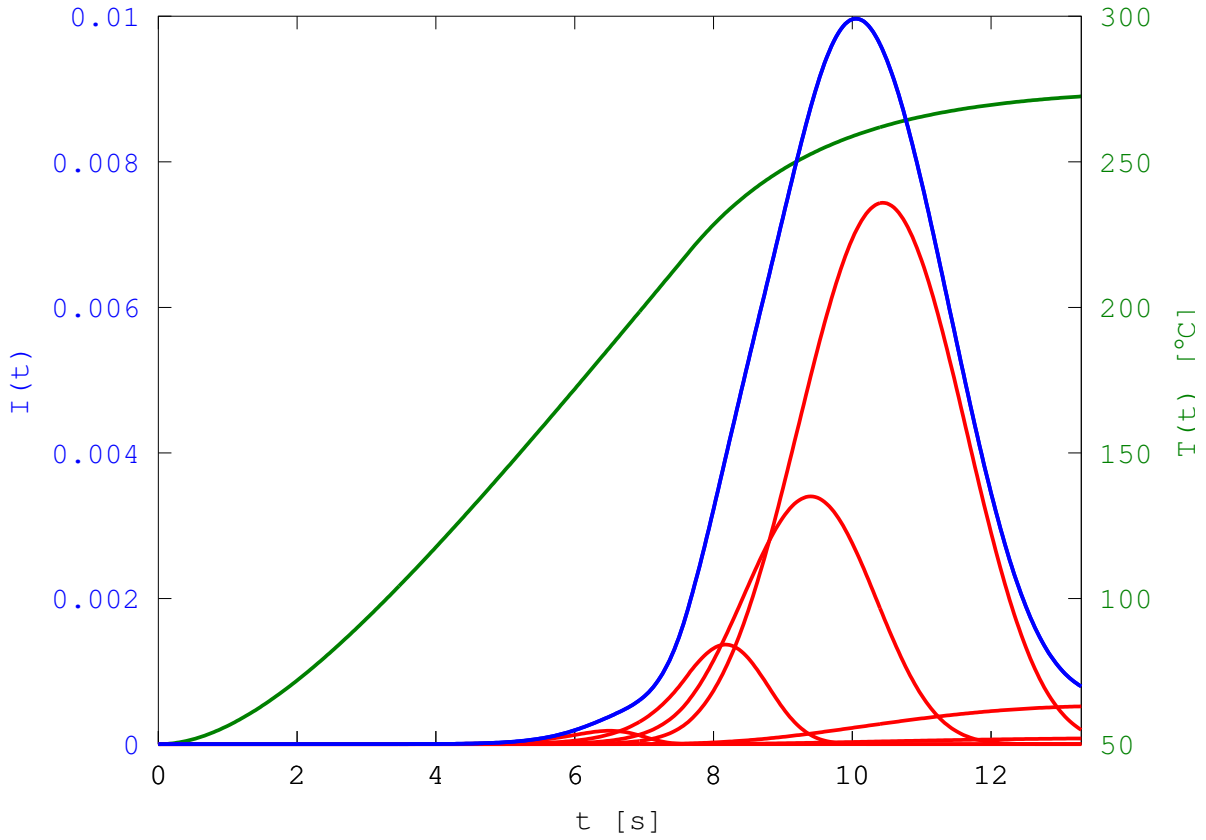

Figure 5.5.: Glow curve simulated with the first order model by Randall and Wilkins (1945a) using the real temperature profile and peaks 2 - 7 from table 2.5. As the heating rate only slowly decreases, the sudden cutoff seen in figure 5.4 does not occur. Instead the glow curve is shifted to later times in the heating profile. This causes the higher peaks to disappear, because the necessary temperatures are reached too late or not at all. If the readout time is increased, the glow curve gradually drops to zero, because the actual heating rate becomes smaller and smaller.

5.1.2. Measured Glow Curves

In the last section it is suggested that a high background is caused by an electron trap from which electrons are only slowly released due to too low temperatures. This was investigated by executing readouts of different duration and maximum temperature on a set of cards with identical doses of 1 Gy. To clear these traps, higher temperatures would be necessary, however, the routine maximum readout temperature can only be slightly increased without damage to the Teflon cover.

The appearance of a glow curve recorded below the maximum temperature of a trap should look the same for different traps. Figures 5.6, 5.7 and 5.8 show what happens when the maximum readout temperature is varied from just above a (shallow) trap at 250 °C over 220 °C to 200 °C. At 250 °C the whole trap is emptied and the peak sharply drops to low values. At 200 °C, however, the peak is smeared out over the whole readout duration. At 220 °C the effect is also already quite pronounced, though the decrease is steeper than at 200 °C. The height decreases with decreasing temperature while the area remains the approximately the same (see table 5.1). This leads to a broadening of the peak and the effect that less and less of the whole area can be covered by a normal readout of a card, which, with only 13.3 s, is just too short.

T_{max} [°C]	Height [nA]	Area [nC]	FWHM [s]	Area I [%]	Figure
250	2239.09	$2.3 \cdot 10^{-4}$	2.7	98.8	5.6
220	1166.74	$2.6 \cdot 10^{-4}$	4.5	77.4	5.7
200	524.52	$2.0 \cdot 10^{-4}$	7.5	53.1	5.8

Table 5.1.: Peak attributes at three different maximum readout temperatures (T_{max}). With decreasing maximum temperature the height (the maximum current of the photomultiplier) decreases while the area (the total amount of charge carriers of the photomultiplier) remains roughly the same. Therefore the full width at half maximum (FWHM) also increases and the peak broadens. This means that less and less of the total area is covered by a readout of normal length (Area I, the left hand side of figures 5.6, 5.7 and 5.8).

As already mentioned, in the case of this trap the temperature of a normal readout is easily high enough to release all electrons. If, however, the trap in question is deeper and requires still higher temperatures than reached during a normal readout, the electrons cannot be released completely without damaging the card. They remain in the trap, get partly released by the next readout and increase the measured dose, thus leading to an increased residual dose on a card. Figures 5.9 and 5.10 show the glow curves of a card with negligible residual dose and a card with increased residual dose. While the main peak is nearly identical (the irradiated dose is 10 mGy for both cards) the end of the glow curve differs: The first card (figure 5.9) drops and remains low while the second card (figure 5.10) starts to rise again at the end. The reason is the high dose of 8 Gy in the previous irradiation of the second card, which led to many electrons being stored at deep, high temperature traps where necessary temperatures to release electrons again are too high.

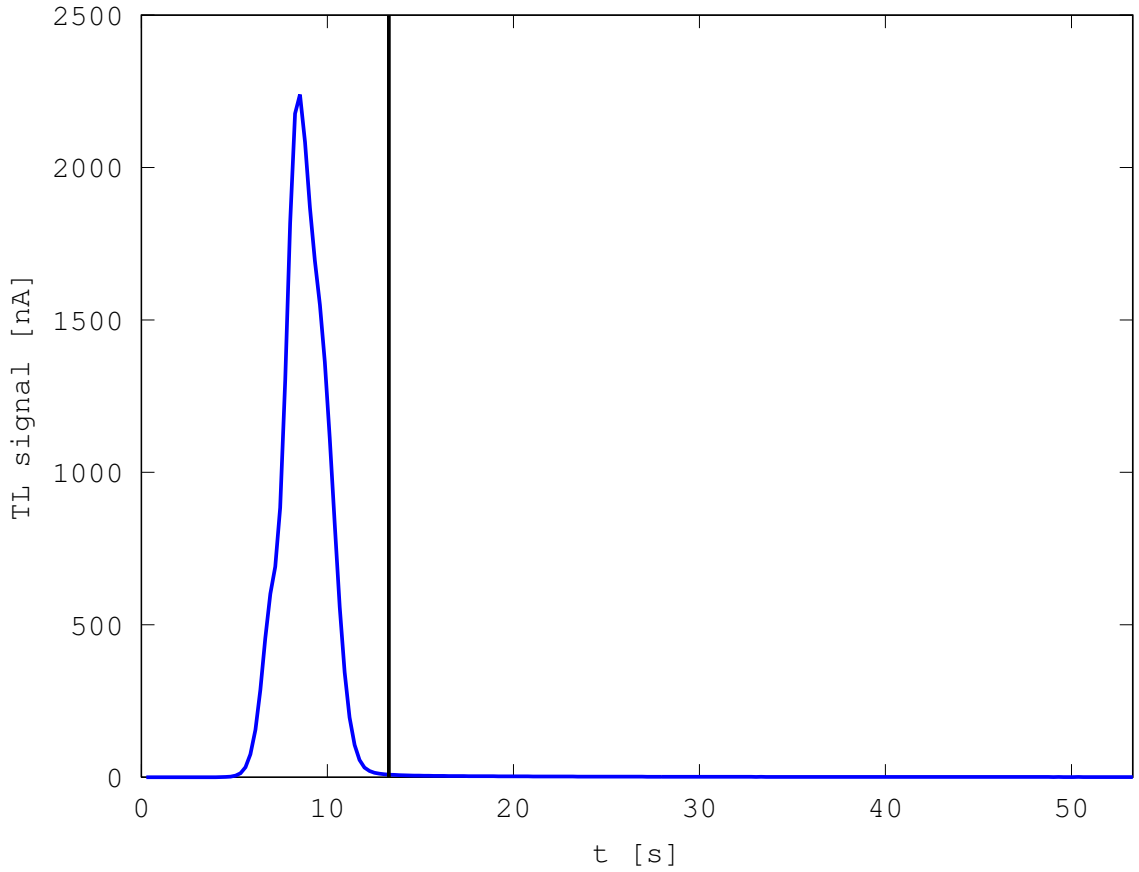

Figure 5.6.: Measured glow curve with a maximum temperature of 250 °C. The glow curve is shown in blue and the duration of a normal readout is marked with a black vertical line at 13.3 s.

Mathematical means of calculation and subtracting an estimation for the residual dose of a card will be discussed in section 5.4.

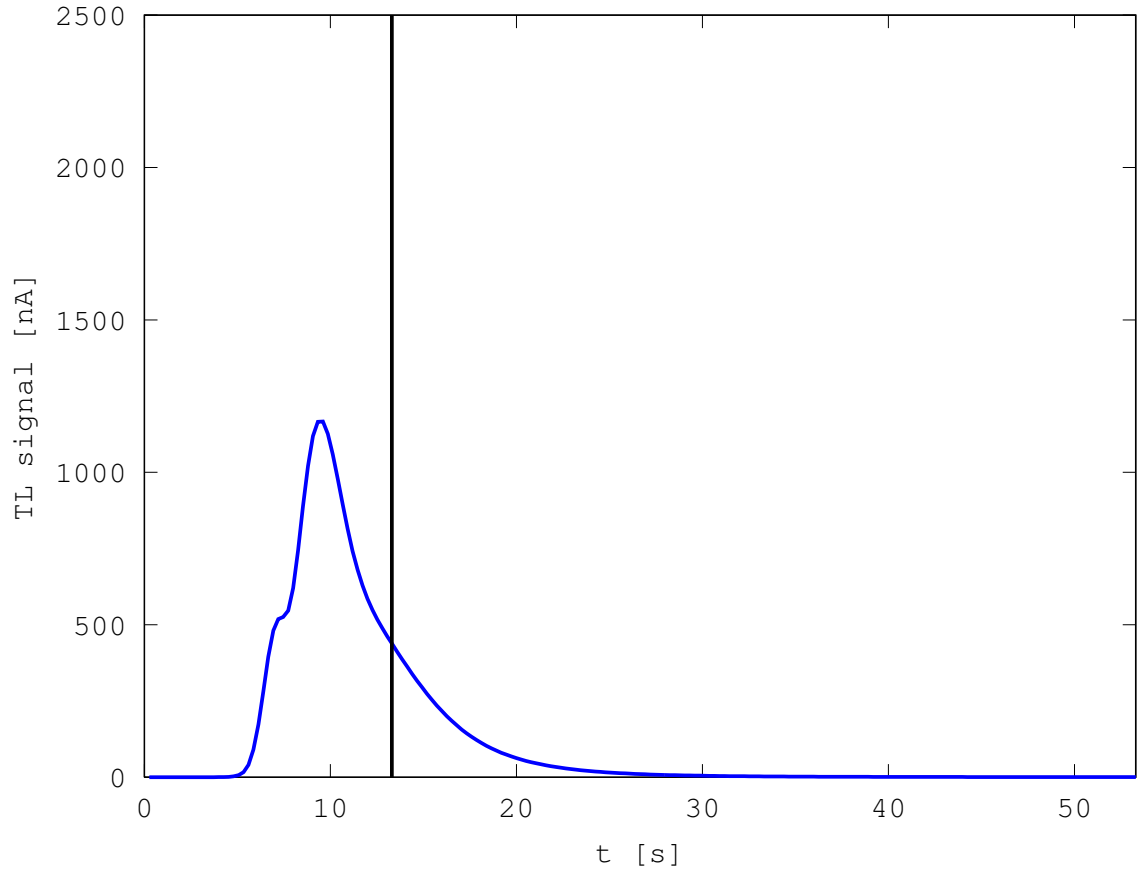

Figure 5.7.: Measured glow curve with a maximum temperature of 220 °C. The glow curve is shown in blue and the duration of a normal readout is marked with a black vertical line at 13.3 s.

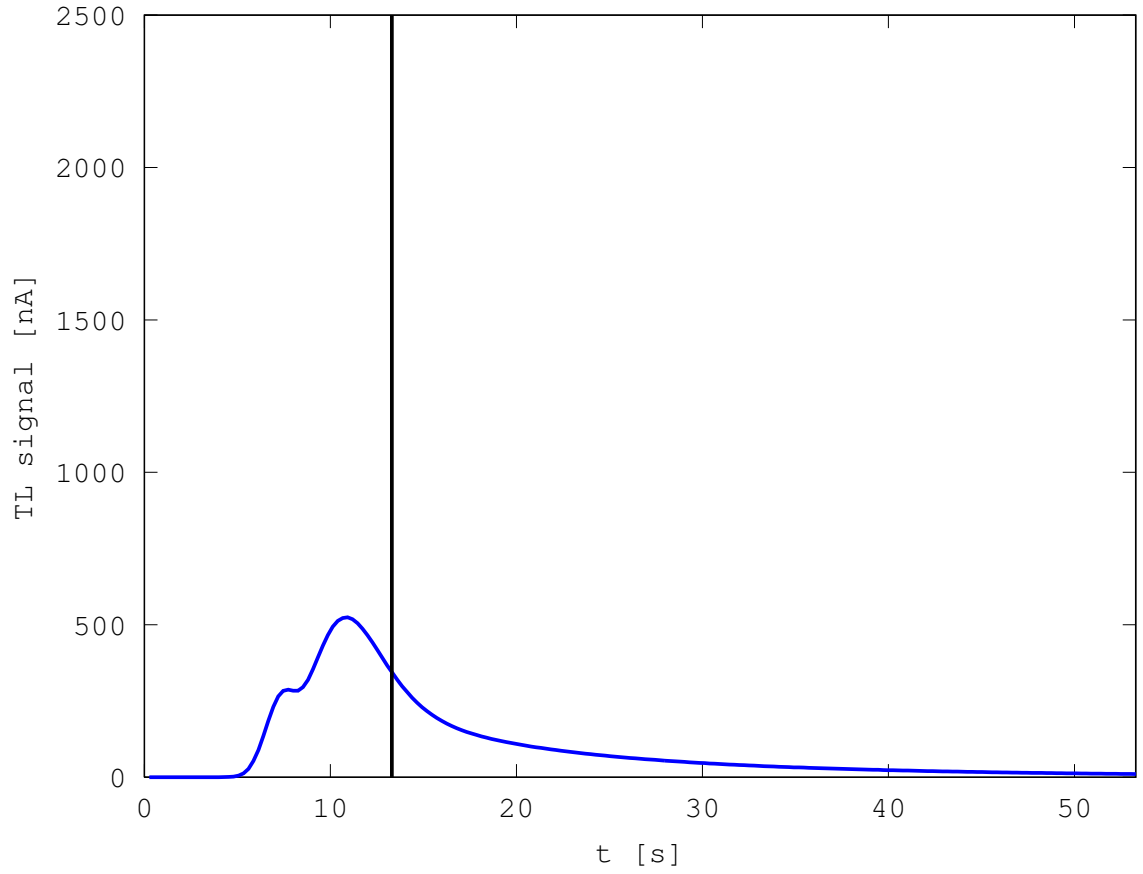

Figure 5.8.: Measured glow curve with a maximum temperature of 200 °C. The glow curve is shown in blue and the duration of a normal readout is marked with a black vertical line at 13.3 s.

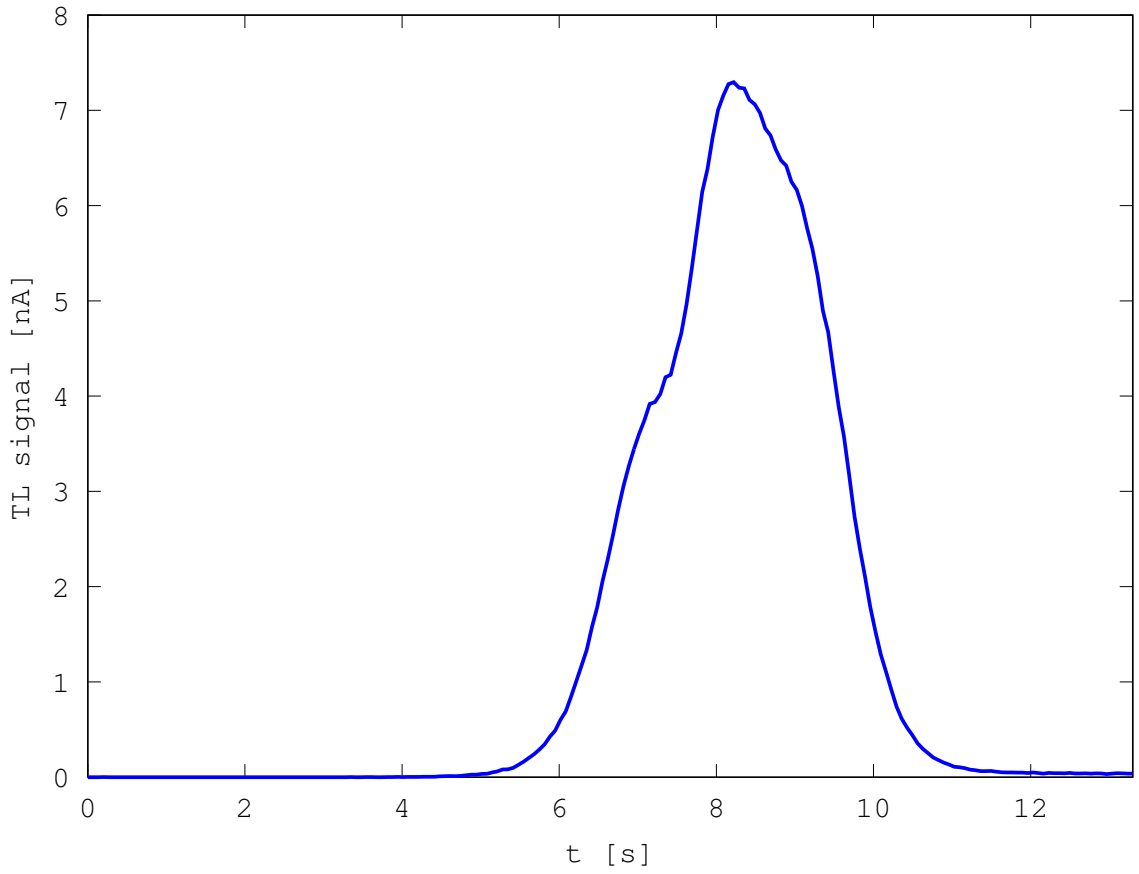

Figure 5.9.: Measured glow curve with a maximum temperature of 280 °C for a card with a negligible residual dose. The duration of the readout is 13.3 s. The irradiated dose for this card is 10 mGy.

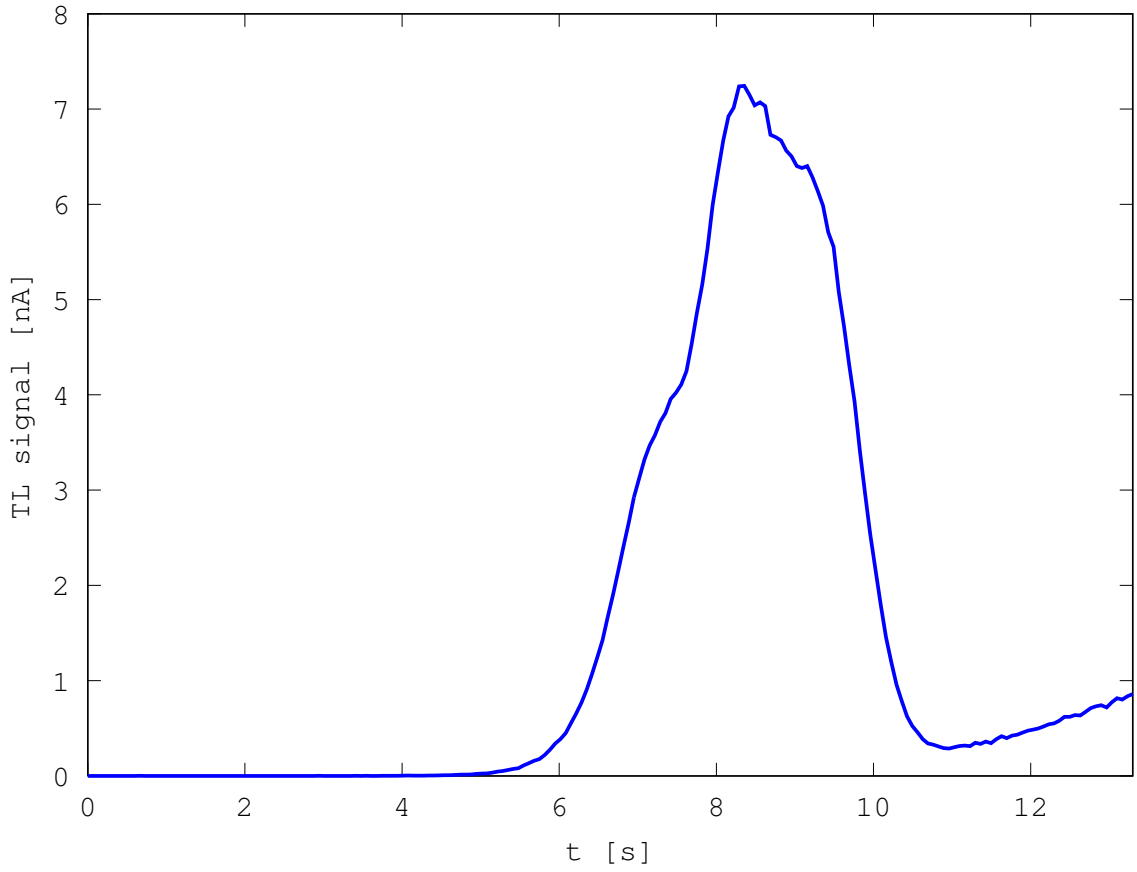

Figure 5.10.: Measured glow curve with a maximum temperature of 280 °C for a card with a high residual dose, visible as a rise at the right hand side. The duration of the readout is 13.3 s. The irradiated dose for this card is 10 mGy and the same as for the card in figure 5.9.

5.2. Wide Dose Range Linearity Measurement

The irradiations that were carried out in the course of this study covered a dose range of 6 orders of magnitude from about 30 μGy up to 20 Gy (for a detailed description of the irradiations see to section 4.4). The aim was to cover the rather small doses occurring in routine dosimetry, which are about the same order of magnitude as the naturally occurring background at the lower range as well as rather high doses of several Gy occurring mainly during radiotherapy. The exact thresholds are defined in IEC 62387-1: measurements need to be possible for a personal dose $H_p(10)$ up to 1 Sv, with an overdose range up to 10 Sv.

Figures 5.11 and 5.12 show the whole range of the measurement. As specified, the linear part stretches up to 1 Gy where the supralinear part (see section 5.3) begins. The whole measurement process follows the outline given in section 4.1. The aim is to investigate the linearity at ideal conditions, therefore the unirradiated transport cards used during this irradiation where used to subtract the natural background. A possible zero-dose is not subtracted for a specific card, but as a mean zero-dose together with the natural background.

The result is that an irradiated dose of 0 Gy should cause the measured dose also to be 0 Gy. A linear fit of the data below 0.01 Gy shows that this is indeed the case. Data above is excluded because of the nonlinearity caused by the onset of supralinearity. The two elements are treated separately and the fit is done according to a simple linear model:

$$D(D_{irr}) = A + B \cdot D_{irr} \tag{5.2}$$

Here, D is the measured dose, D_{irr} the irradiated dose and the two constants A and B are the y-intercept (or the zero-dose) and the slope. For a perfectly linear behaviour A should be 0 and B should be 1, therefore, the measured dose should equal the irradiated dose and at an irradiated dose of 0 Gy no dose should be measured. Table 5.2 shows the parameters obtained by the fit. Parameter B is approximately 1. The negative values for A of course do not make sense but they suggest that the natural background which was subtracted was chosen too high.

Element	A [μGy]	B
2	-21$\pm$7	1.007$\pm$0.002
3	-11$\pm$9	1.007$\pm$0.002

Table 5.2.: Parameters obtained for a linear fit (equation 5.2) of doses below 0.01 Gy after a background dose calculated from unirradiated cards has been subtracted.

This is underlined when the fit is repeated with no background correction: Positive values are obtained for parameter A while parameter B remains approximately 1 (see table 5.3 and figures 5.13 and 5.14).

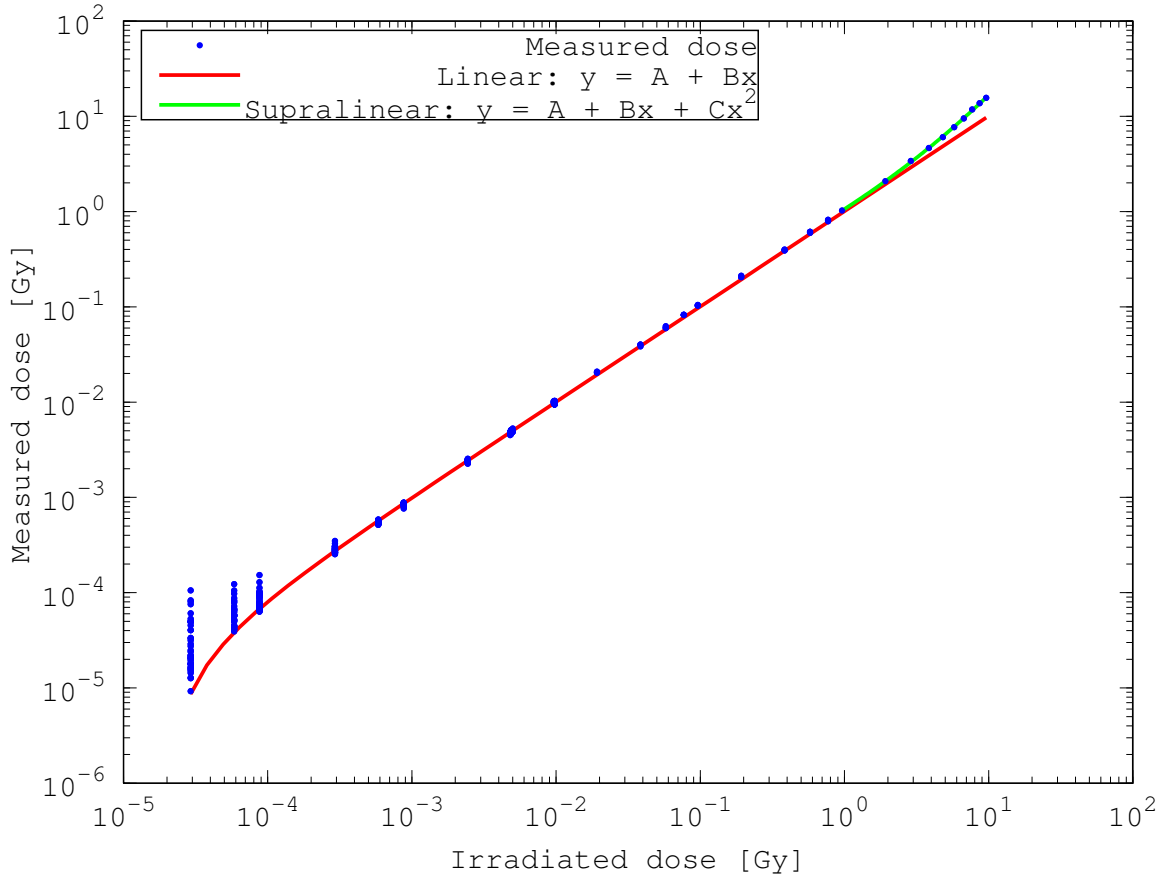

Figure 5.11.: Measured dose as a function of the irradiated dose. Long range linearity measurement with transport correction for element 2. The background that was subtracted was obtained from unirradiated transport cards. The data (blue dots) is used for a linear fit (red line) for doses below 0.01 Gy and for a quadratic fit (green line) for the supralinear part and doses above 1 Gy. The parameters and errors are given in table 5.2. The supralinear part is discussed further in section 5.3.

Element	A [μGy]	B
2	8±7	1.001±0.002
3	18±9	1.001±0.002

Table 5.3.: Parameters obtained in a linear fit (equation 5.2) of doses below 0.01 Gy without any background correction.

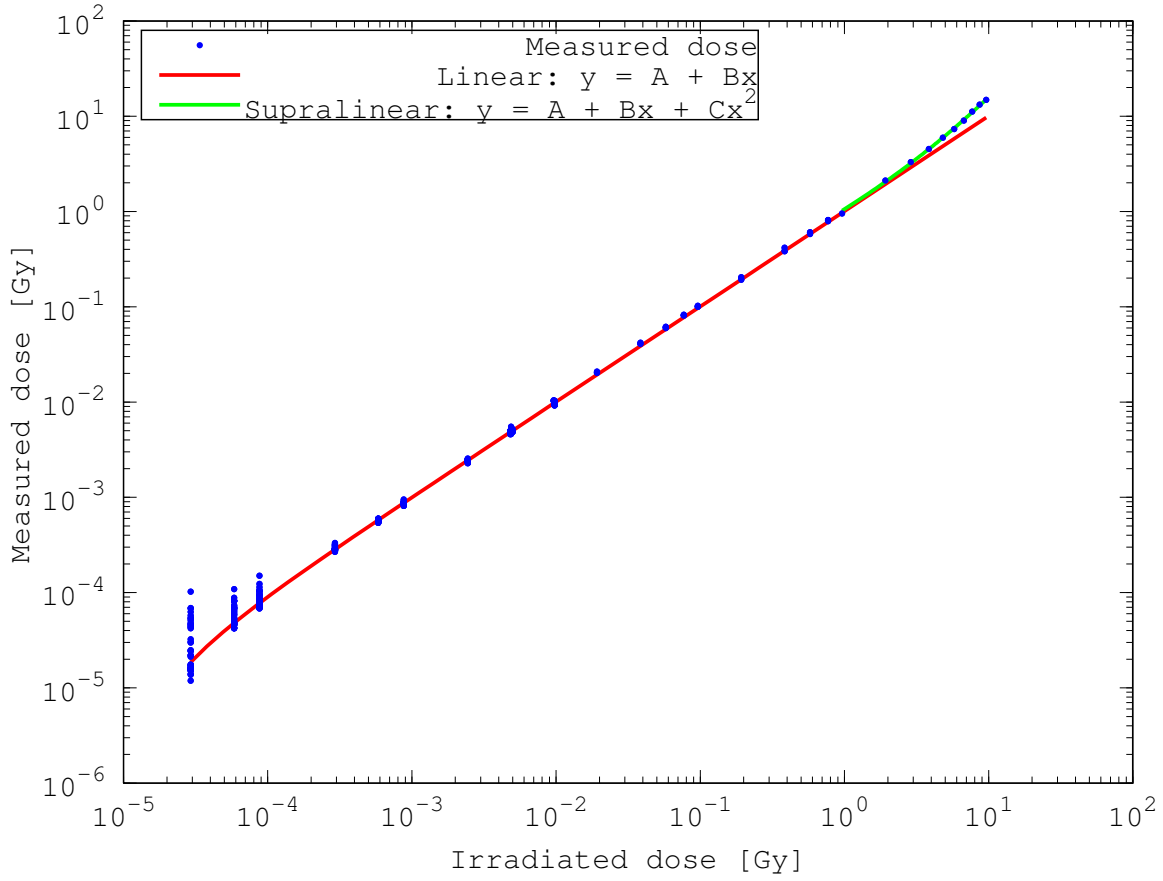

Figure 5.12.: Measured dose as a function of the irradiated dose. Long range linearity measurement with transport correction for element 3. The background that was subtracted was obtained from unirradiated transport cards. The data (blue dots) is used for a linear fit (red line) for doses below 0.01 Gy and for a quadratic fit (green line) for the supralinear part and doses above 1 Gy. The parameters and errors are given in table 5.2. The supralinear part is discussed further in section 5.3.

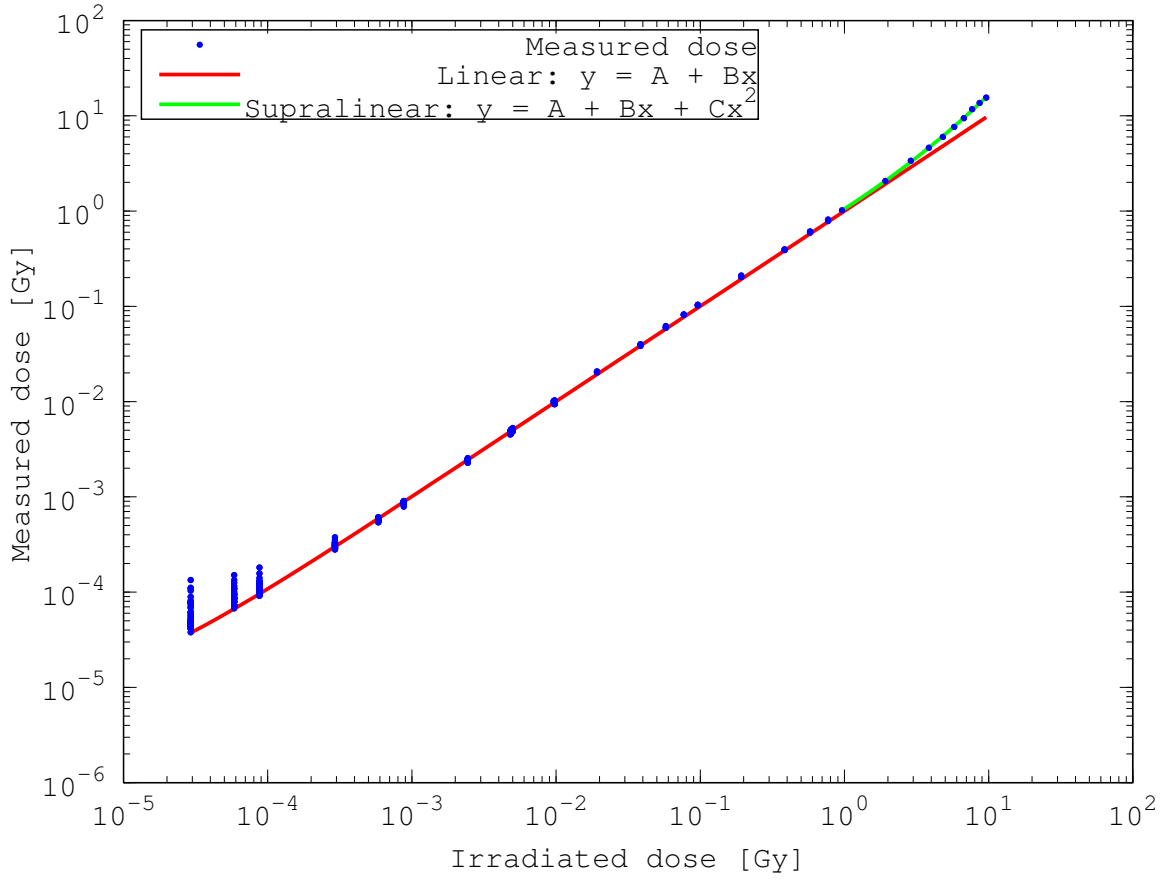

Figure 5.13.: Long range linearity measurement without background subtraction for element 2. The data (blue dots) is used for a linear fit (red line) for doses below 0.01 Gy and for a quadratic fit (green line) for the supralinear part and doses above 1 Gy. The parameters and uncertainties are given in table 5.3. The supralinear part is discussed further in section 5.3.

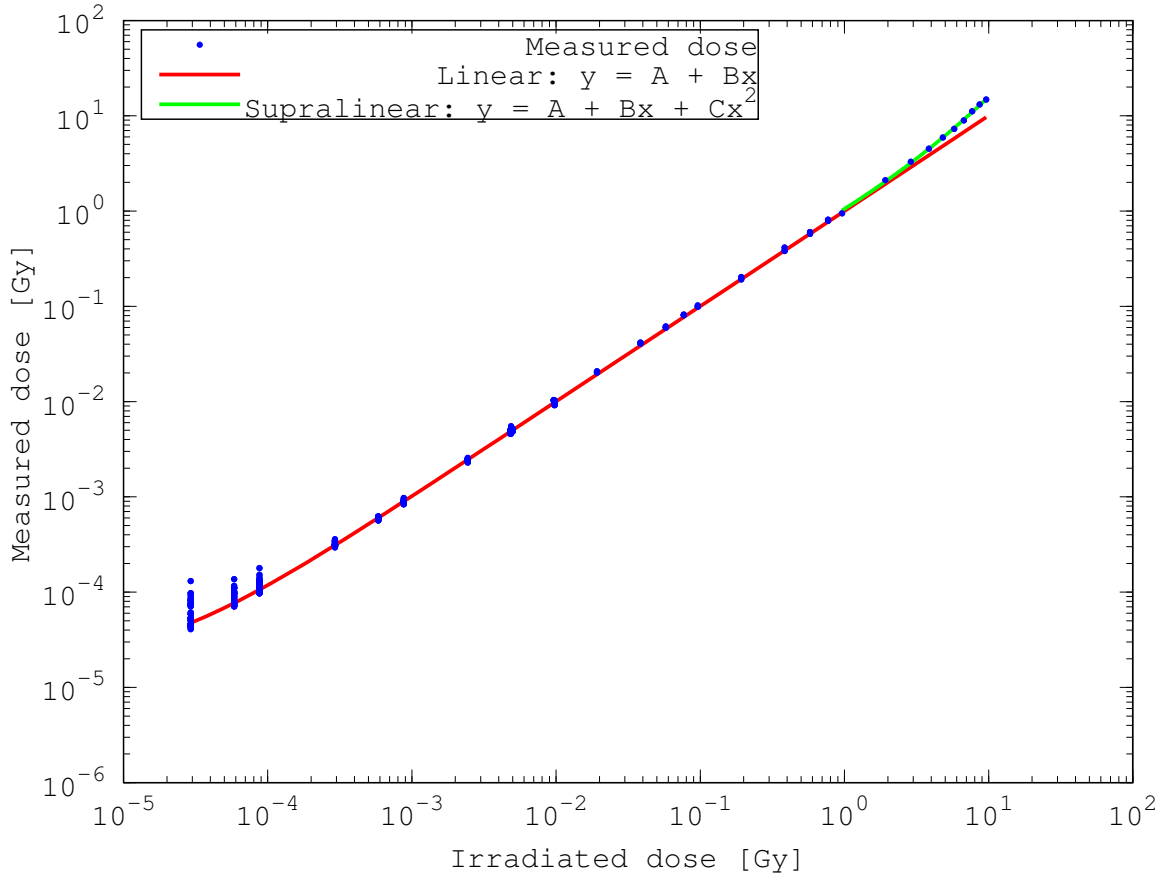

Figure 5.14.: Long range linearity measurement without background subtraction for element 3. The data (blue dots) is used for a linear fit (red line) for doses below 0.01 Gy and for a quadratic fit (green line) for the supralinear part and doses above 1 Gy. The parameters and uncertainties are given in table 5.3. The supralinear part is discussed further in section 5.3.

5.3. Supralinearity

As mentioned in the previous section concerning the linear range, the supralinear part becomes important at doses higher than about 1 Gy. Figures 5.15 and 5.16 show the region from 1 Gy upwards together with the linear fit from the previous section and a quadratic fit based on equation 5.3 for the supralinear part for elements 2 and 3 respectively.

$$D(D_{irr}) = A + B \cdot D_{irr} + C \cdot D_{irr}^2 \tag{5.3}$$

This equation can be inverted:

$$D_{irr} = \frac{\sqrt{B^2 - 4AC + 4CD_{measured}} - B}{2C} \tag{5.4}$$

The correction in equation 5.4 can then be applied to doses in the supralinear dose range, that is for doses greater than 0.8 Gy. Below this threshold no correction needs to be applied.

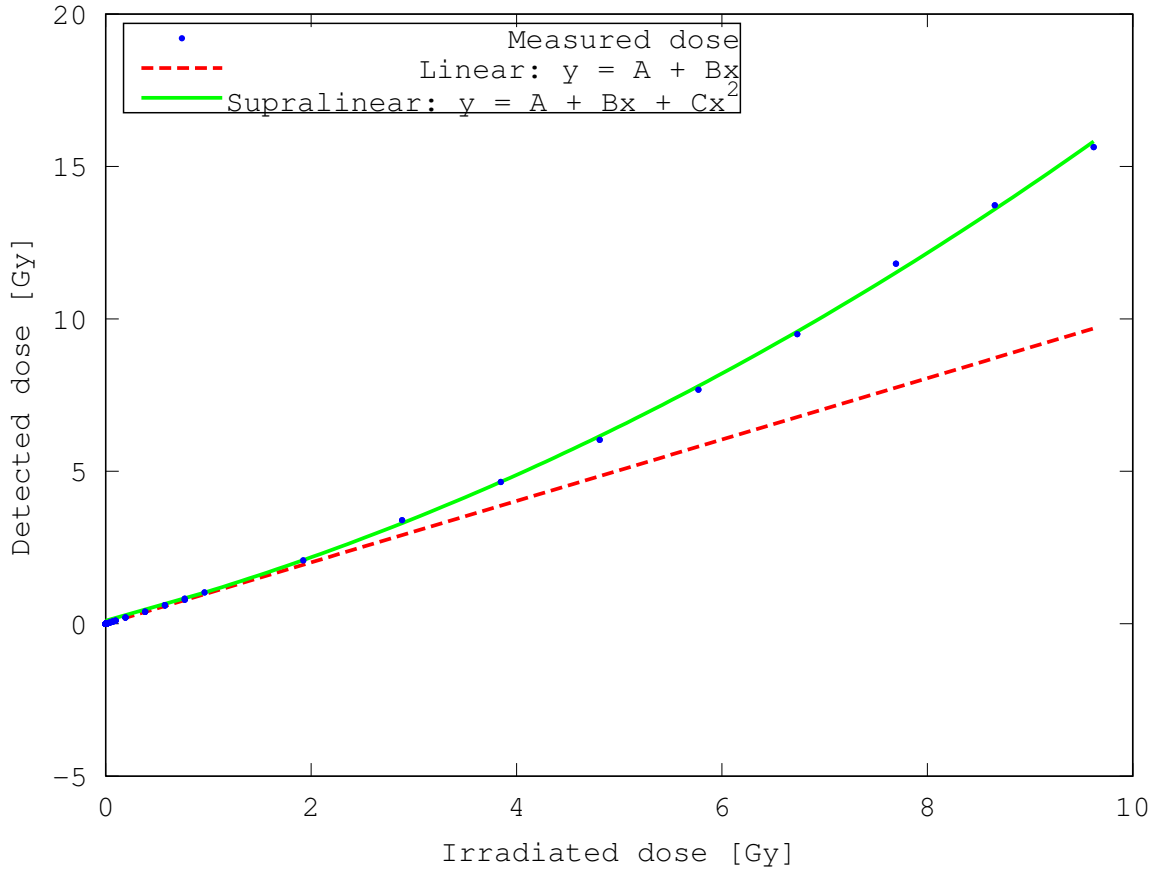

Figure 5.15.: Quadratic fit of supralinear range with transport correction for element 2. The linear fit (dashed red line) is extended across the supralinear range. The quadratic fit of the supralinear part is shown in green. The parameter of the quadratic fit are given in table 5.4.

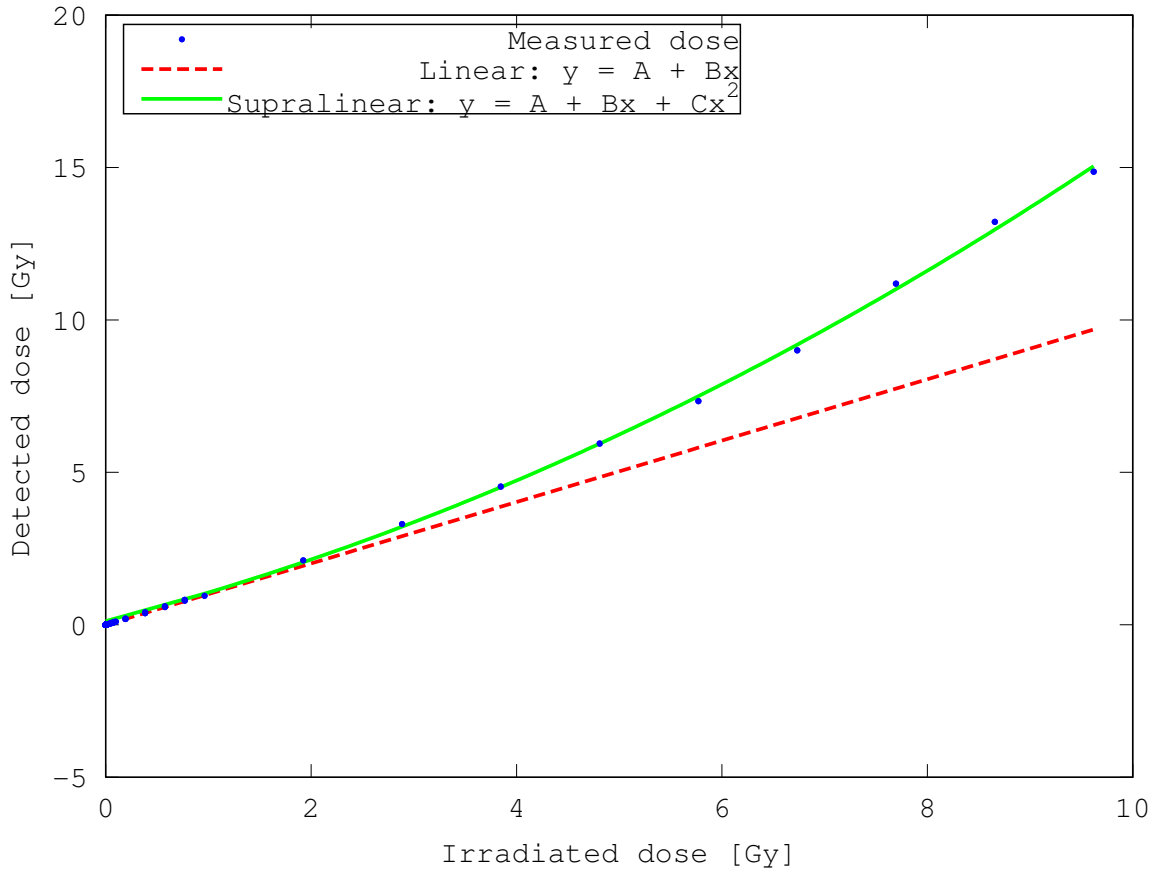

Figure 5.16.: Quadratic fit of supralinear range with transport correction for element 3. The linear fit (dashed red line) is extended across the supralinear range. The quadratic fit of the supralinear part is shown in green. The parameter of the quadratic fit are given in table 5.4.

Element	A [Gy]	B	C [Gy^{-1}]
2	0.1±0.2	0.88±0.08	0.078±0.008
3	0.1±0.2	0.87±0.09	0.071±0.008

Table 5.4.: Parameters of the quadratic fit (equation 5.3) obtained with the least-squares method.

5.4. Residual Dose Correction

An effect that was already mentioned in section 5.1 is the lingering effect of irradiations with high doses. The limited temperature during the readout process enables a part of the electrons stored at high temperature traps to remain there. At the next readout, a part of these electrons is also released, together with electrons added to traps due to possible additional radiation captured by the dosimeter and electrons that spontaneously decayed to lower energy traps. The electrons that were stored because of the original high dose irradiation continue to influence later measurements. This, so far, is shown in the glow curves that were simulated and measured in section 5.1 and can be seen as the dose dependent part of the residual dose of a card.

The second part making up the residual dose is the material dependent zero-dose, which occurs during all dose readouts. It is usually in the order of several μGy and can be measured by reading out a completely empty dosimeter.

There is therefore a constant and a variable part, which together produce the residual dose of a dosimeter. While the constant part is assumed to be the same during consecutive measurements, the variable part is further and further decreased with each measurement.

5.4.1. Reread

The residual dose appears for example during a reread, which is a second readout procedure done immediately following a previous one.

In routine dosimetry a reread is carried out automatically if the measured dose of an element exceeds 150 μGy, to ensure the dosimeter is emptied and ready to use again. Mason et al. (1977) already used the reread together with ultraviolet light bleaching to re-estimate the previously absorbed dose. This is also possible the other way round, i.e., from a known irradiation it is possible to estimate the dose value of the reread.

The relation between an original read and its readout has been investigated and the results are shown in figures 5.17 and 5.18 for elements 2 and 3 respectively.

A linear fit (see equation 5.5) has been used for doses below 1 Gy (the onset of supralinearity, see section 5.3), which yielded the parameters given in table 5.5. The very small parameter b means that the linear part becomes negligible compared to the constant parameter a at small doses. At higher doses (where the parameter a becomes in turn negligible compared to the dose) this corresponds to a reread of, for example, (1.67$\pm$0.01) ‰ of the original dose for element 2.

$$D_{reread} = a + b \cdot D_{original} \tag{5.5}$$

Element	a [μGy]	b
2	6$\pm$1	(1.67$\pm$0.01)$\cdot 10^{-3}$
3	8$\pm$1	(1.73$\pm$0.01)$\cdot 10^{-3}$

Table 5.5.: Parameters obtained for a linear fit of the reread for doses below 1 Gy.

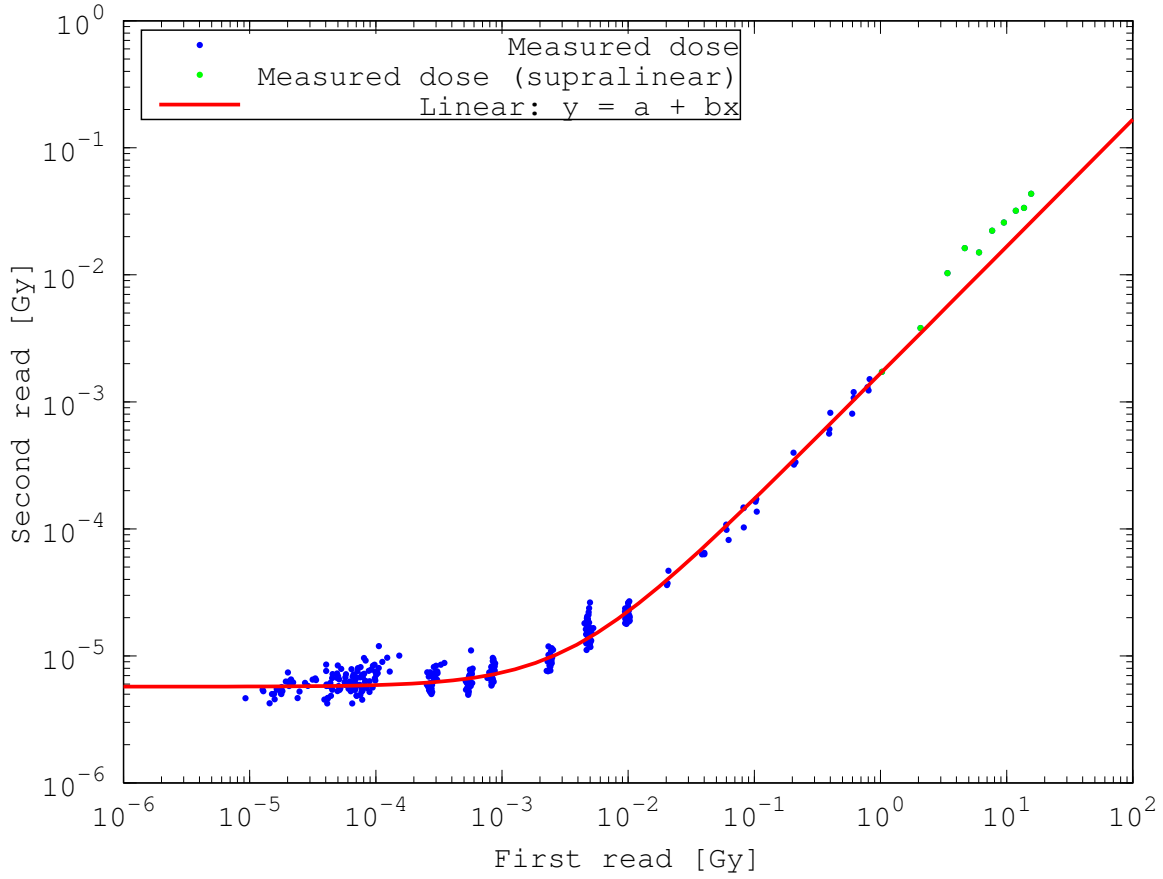

Figure 5.17.: Dependence of dose value of the second readout (the reread) on dose value of the first readout for element 2. The data (blue dots) has been used for a linear fit (red). The data measured in the supralinear range (green dots) was excluded from the fit. See table 5.5 for the fitting parameters.

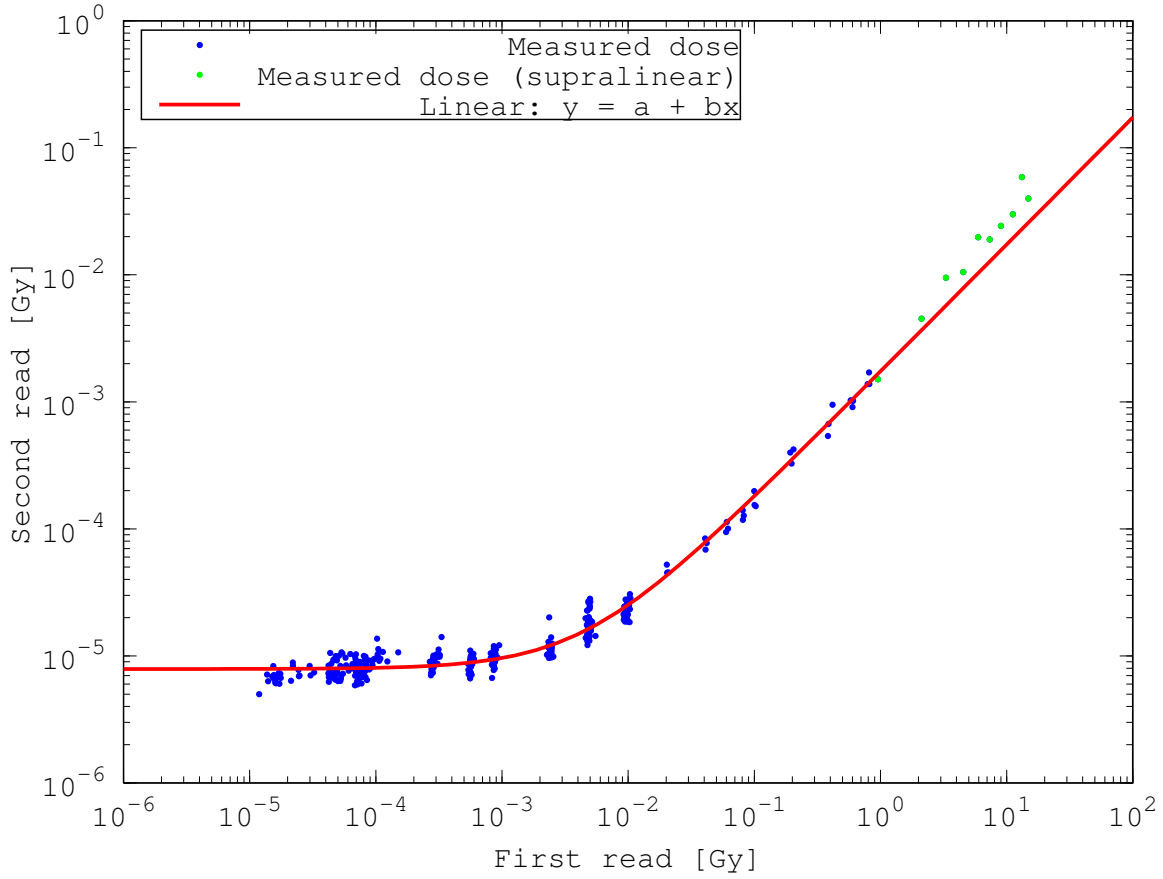

Figure 5.18.: Dependence of dose value of the second readout (the reread) on dose value of the first readout for element 3. The data (blue dots) has been used for a linear fit (red). The data measured in the supralinear range (green dots) was excluded from the fit. See table 5.5 for the fitting parameters.

Therefore, a fast way to find out if a card has an increased residual dose and should possibly be discarded is to check whether the reread is above a certain threshold.

Another deduction that can be made is the fact that even an irradiated dose of 0 Gy apparently would lead to a non-zero reread. This is seen when executing consecutive readouts: as the card has been completely emptied a few seconds before by the previous readout procedures and no irradiations occurred since then, the measured dose should be zero. This is in part caused by a dark current from the photomultiplier. The dark current for each detector is automatically calculated at the beginning of each readout procedure. Table 5.6 gives the dark current for each element, which is about half of the zero-dose.

Element	Dark current [μGy]
2	2.1$\pm$0.8
3	4.1$\pm$0.8

Table 5.6.: Dark current of element 2 and 3. This is approximately half of the zero-dose.

Furthermore, the dose measured in consecutive readouts decreases, but only until a constant dose is reached. Different cards have different zero-doses as well as a different rate at which the residual dose decreases. For simplicity, the residual dose was defined to include the zero-dose and not decay to zero but to the constant zero-dose. Together, they can be modeled by an exponential decay (see equation 5.6).

The conclusion is that the amount of irradiated dose has an influence on the residual dose stored on a card. This residual dose can be reduced by several additional readouts, and completely erased if it is small enough or the card is subjected to a sufficient number of readouts. The residual dose can be subtracted to decrease the influence from a card specific zero-dose on one hand and the influence of previous irradiations on the other.

To prove that this is indeed sensible three methods of residual dose reduction have been devised and tested:

1. The Simple Reread Method
2. The Linear Method
3. The Exponential Method

In the simple reread method the reread is subtracted from the originally measured dose. This method is very easy to add to the existing routine, as a reread is already done automatically for doses above 150 μGy.

The linear method makes use of the first and the second reread. The two dose values are used for a linear interpolation back to the original read, which can then be subtracted. This method would require an additional reread to be executed.

The exponential method makes use of the exponential decay of the rereads. The following function is used to model the decrease:

$$RD(k) = A + Be^{-Ck} \tag{5.6}$$

Here, $RD(k)$ is the residual dose after k readouts, A is the constant zero-dose and B and C are constants that describe the decrease. For a large number of rereads the second summand becomes smaller and smaller, thus being dominated by the constant zero-dose A. This simulates the elimination of the residual dose by a sufficiently large number of rereads.

To model this exponential decrease the three constants have to be determined. This was done by analysing up to 9 rereads of 457 cards. The investigation showed that high reread values are usually really just temporarily increased and that setting the constant A to a small zero-dose greatly increased the accuracy of the fit. Ideally this would mean determining the material dependent zero-dose for each card before use, for example by reading out the cards several consecutive times until the reread does not decrease any further. For this evaluation the value of the constant a as calculated in section 5.4.1 and given in table 5.5 has been used for all cards.

The constant B has values in the same order of magnitude as the constant A for cards with a negligible residual dose. An increased residual dose can lead to significantly higher values in the order of several thousand μGy. B is therefore a rough indication of the residual dose.

The constant C indicates how fast the residual dose is decaying, with higher values indicating a quicker decay. It was limited to values in the range of 10^{-6} to 3 for practical reasons and to ensure stability. The upper bound was chosen because in the case of $C = 3$ it already takes less than one reread to remove the residual dose, higher values are therefore not necessary. The lower bound is chosen greater than zero to ensure stability of the fit.

Figures 5.19, 5.20 and 5.21 show the results of three exponential fits for cards with low, medium and high residual dose respectively. The parameters for the fits are given in table 5.7.

Residual dose	Element	A [μGy]	B [μGy]	C
low	2	6±1	1.79±0.07	1.3±0.2
	3	8±1	2.6±0.1	0.53±0.2
medium	2	6±1	27±1	0.597±0.002
	3	8±1	29±2	0.537±0.002
high	2	6±1	1013±8	0.039025±0.000002
	3	8±1	916±10	0.049031±0.000002

Table 5.7.: Parameters obtained for an exponential fit (equation 5.6) of dose values of the rereads of three different cards with a low, medium and high residual dose.

Once the constants have been determined it is possible to calculate the number of rereads for which the residual dose decreases below a certain dose level L:

$$k(L) = \frac{1}{C} \ln \frac{B}{L - A} \tag{5.7}$$

Here, L is the level of residual dose to be reached and $k(L)$ the number of rereads necessary to achieve this. For demonstration, the value for L is set to 25 μGy, though a residual dose of less than 15 μGy would be required, if the dosimeter were to be used for

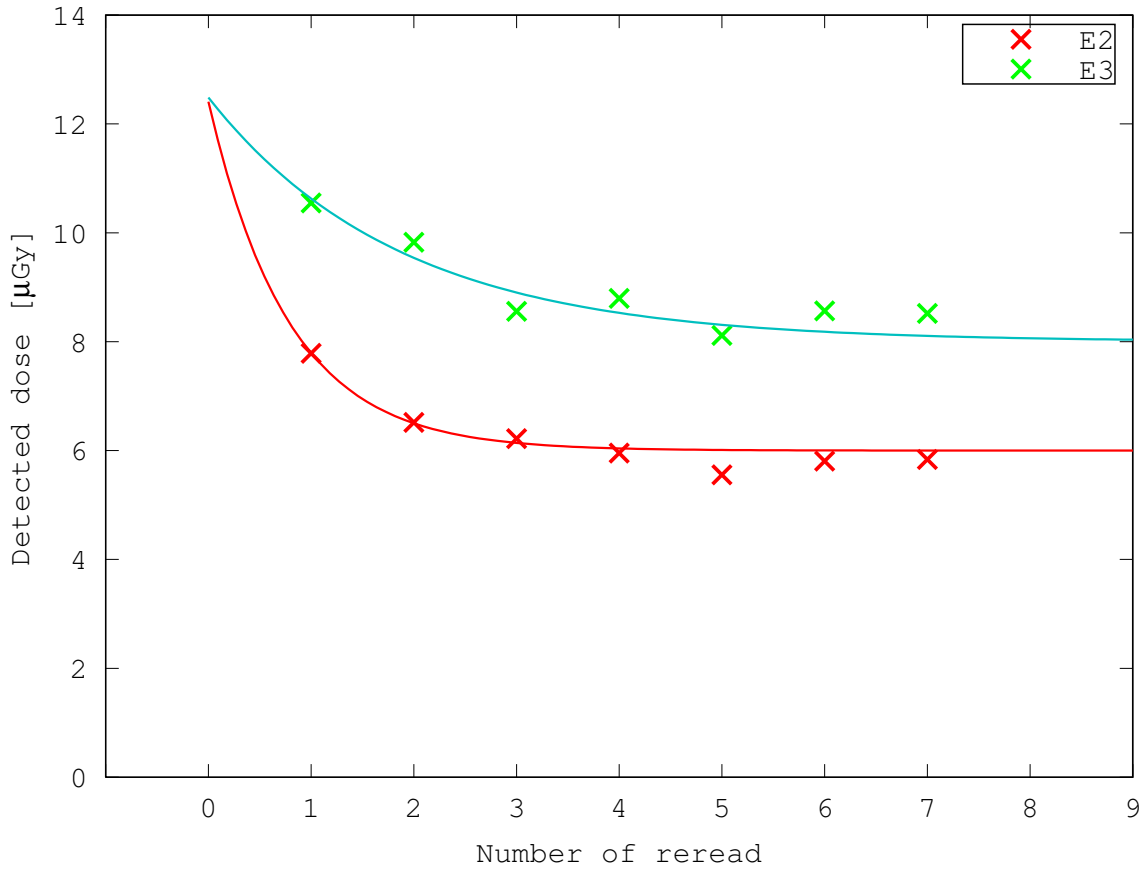

Figure 5.19.: Exponential fit of the dose values of the rereads for element 2 and 3 of a card with a low residual dose. The parameters of all displayed fits are given in table 5.7.

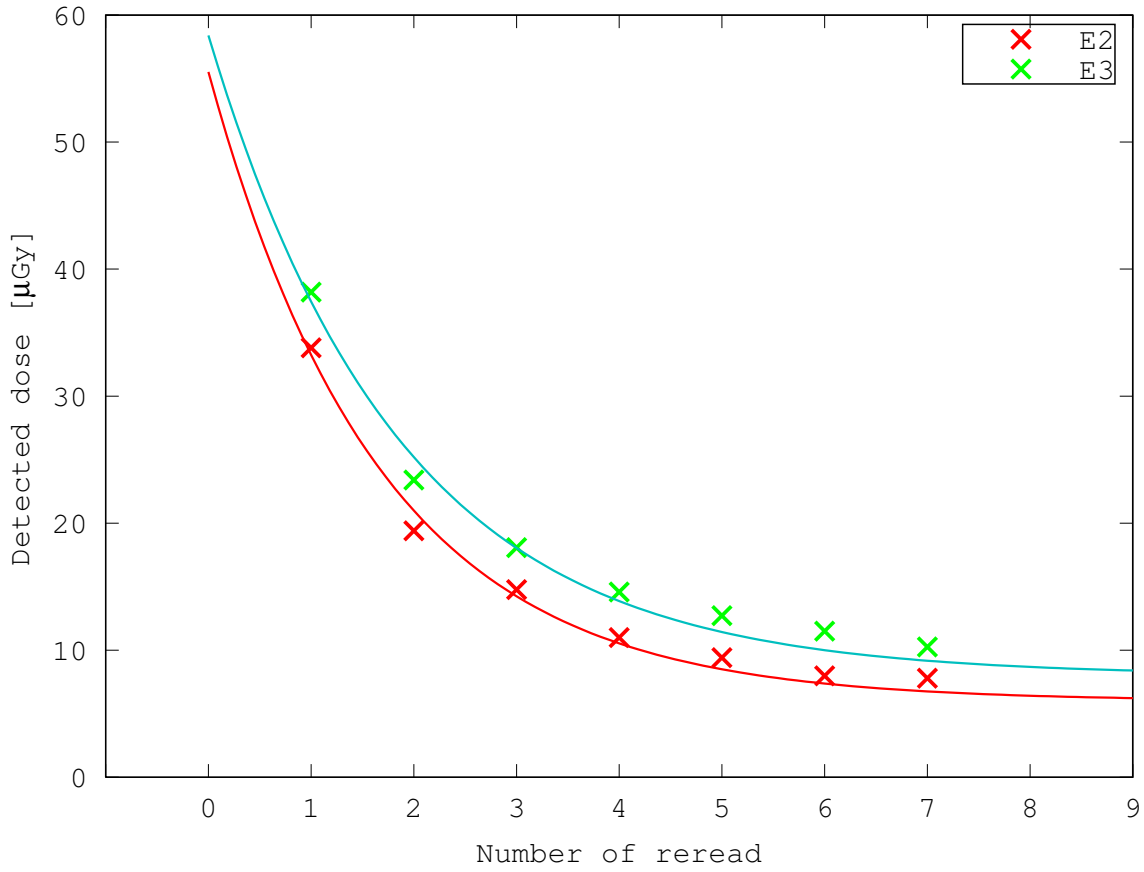

Figure 5.20.: Exponential fit of the dose values of the rereads for element 2 and 3 of a card with a medium residual dose. The parameters of all displayed fits are given in table 5.7.

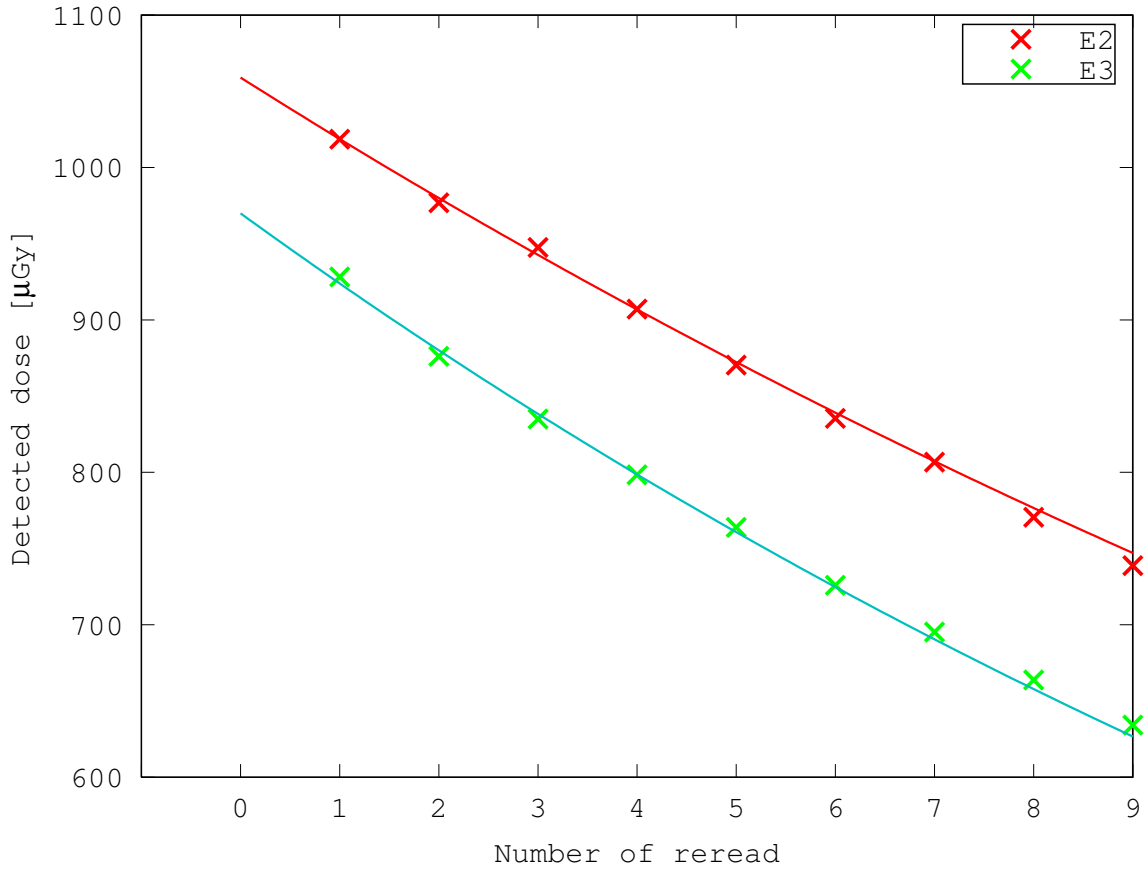

Figure 5.21.: Exponential fit of the dose values of the rereads for element 2 and 3 of a card with a high residual dose. The parameters of all displayed fits are given in table 5.7.

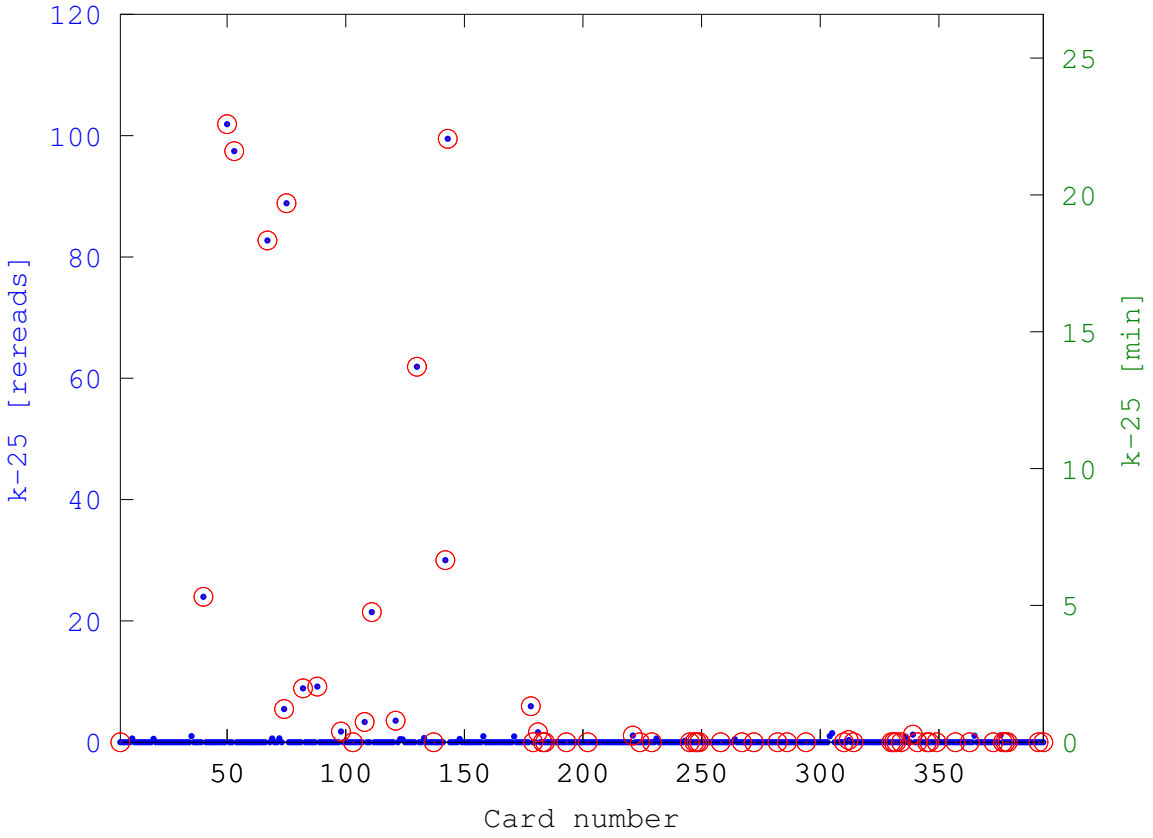

Figure 5.22.: Number of rereads necessary to decrease the residual dose below 25 μGy for element 2 of all cards used in this thesis. The defect cards (see section 4.4, table 4.2) are marked with a red circle, as only these were used for irradiations with high doses. They correspond to the cards which need a high number of rereads to be returned to normal residual dose levels.

routine dosimetry. If the residual dose is already below L this will yield negative results, in which case no further rereads are necessary. Figures 5.22 and 5.23 show the number of rereads (and the corresponding time in minutes) necessary to reach a residual dose of 25 μGy for the cards used and irradiated during this thesis. It can be seen that several cards would need approximately 100 rereads to return to the normal residual dose levels. The cards in question were irradiated with doses above 1 Gy. These cards are defect cards (as described in section 4.4) and therefore marked with a red circle in figures 5.22 and 5.23. The cards for which the exponential decay of the dose values of the rereads was demonstrated had previously been irradiated with 7 Gy (high residual dose), 580 μGy (medium residual dose) and 90 μGy (low residual dose).

The cards used for the fit examples in figures 5.19, 5.20 and 5.21 have values of $k(25)$ as given in table 5.8.

Whereas the cards with a low or medium residual dose can be restored to a level below

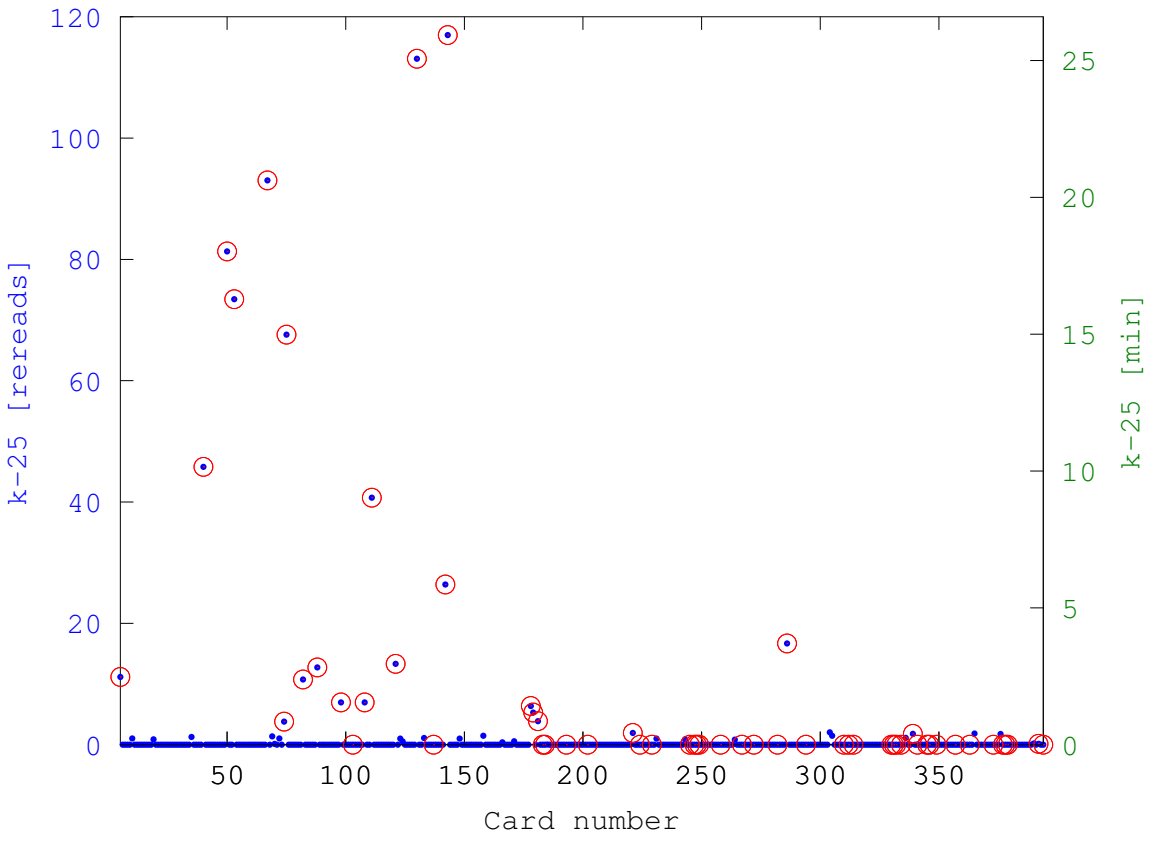

Figure 5.23.: Number of rereads necessary to decrease the residual dose below 25 μGy for element 3 of all cards used in this thesis. The defect cards (see section 4.4, table 4.2) are marked with a red circle, as only these were used for irradiations with high doses. They correspond to the cards which need a high number of rereads to be returned to normal residual dose levels.

	low	medium	high
Element 2	0±0.4	0.6±0.2	101±2
Element 3	0±0.3	1±0.2	81±1

Table 5.8.: Number of rereads necessary to decrease the residual dose below 25 μGy for the three cards shown in figures 5.19, 5.20 and 5.21. The card with the low residual dose is already below that threshold. The card with a medium residual dose will fall below 25 μGy after one reread while the card with the high residual dose requires either 81 or 101 rereads for element two or three.

25 μGy with just one reread the card with a high residual dose requires either 81 or 101 rereads for element 2 or 3. To perform 100 separate rereads takes about 22 minutes though a lot of time is spent first on letting the cards cool down to the preset initial temperature and then on heating to maximum temperature again. As indicated by figure 5.2 only after 60 % (or 9 seconds) of the readout time 90 % of the maximum temperature is reached. Therefore, if the deletion was done in one continuous heating cycle the necessary time could be decreased significantly. However, as this puts a lot of stress on both the card and the reader it is not advisable.

Furthermore, it is not necessary anymore to completely erase the card, as we know the function with which the residual dose is going to decrease on further readouts.

5.4.2. Comparison of the Methods

The methods can be compared concerning two criteria: applicability and quality.

Applicability

All methods require the execution of additional rereads. For measured doses exceeding 150 μGy a reread is already automatically done in routine. However, doing a reread on every readout procedure would of course roughly double the necessary time. Whether this is feasible depends on the number of cards in use, or rather the number of cards that have to be evaluated every month.

For the first method a possible application would be to use the reread only when one is already done, that is for doses exceeding 150 μGy. Therefore, for smaller doses the original procedure is kept, where a blank value of 25 μGy is subtracted (see section 4.1), while for greater doses the respective value of the reread is subtracted as an individual residual dose.

For the second method, where two rereads are required, applies the same.

For the third method the case is different: Here, with two parameters that have to be determined to model the residual dose, at least two rereads are necessary, with the fit being more accurate if more rereads are available. However, the resulting function allows to calculate the residual dose of a card in advance and to predict the value of future rereads. This is of great value when the card in question has an exceptionally high residual dose due to irradiations with very high doses (several Gy). This is the case, e.g., for the card with

the high residual dose from the previous section. As mentioned there, the residual dose is too high to be effectively erased, but as it can be calculated for future readouts according to equation 5.6, these can be adapted accordingly to correct the increased residual dose.

Quality

All three methods change the originally measured dose by subtracting a differently calculated residual dose. For the investigation of the quality of each method the corrected doses were compared to the known irradiated doses via the dose response:

$$F(D_{irradiated}) = \frac{D_{measured}}{D_{irradiated}} \tag{5.8}$$

In the ideal case the dose response should be 1 over the whole linear range. In the case of an increased residual dose the dose response would be greater than 1, as the measured dose $D_{measured}$ is higher than the irradiated dose $D_{irradiated}$. When the residual dose correction is applied in the form of one of the three methods mentioned above, these cases should be corrected, i.e., the dose response should be closer to 1 after the correction. A good method should therefore subtract a high enough amount where necessary but of course not too much for cards with a normal or negligible residual dose.

As a measure for the quality the difference between the dose response and 1 is used, as defined in the following by the parameter Q:

$$Q = \sqrt{\sum_k (F_2(D_k) - 1)^2} + \sqrt{\sum_k (F_3(D_k) - 1)^2} \tag{5.9}$$

Where k is the card number of which the dose response F_i is calculated for element i, two and three. The quality parameter Q is calculated before the residual doses correction and after the application of each method. As the amount of cards does not change and the cards are divided in routine cards and defect cards (see table 4.2 in section 4.4), Q is normalized with respect to the number of cards N, depending on whether the routine, defect or all cards are compared (equation 5.10).

$$q_i = \frac{Q_i}{N_i} \tag{5.10}$$

Method	q_{All}	q_{Defect}	$q_{Routine}$
none	0.01981 (100%)	0.12941 (100%)	0.00671 (100%)
Reread	0.00530 (26.8%)	0.01591 (12.3%)	0.00557 (83.0%)
Linear	0.00518 (26.1%)	0.01498 (11.6%)	0.00550 (82.0%)
Exponential	0.00484 (24.4%)	0.01556 (12.0%)	0.00501 (75.1%)

Table 5.9.: Normalised quality parameter q (equation 5.10) for each method of residual dose correction and card group.

A second indicator for the quality of a method is whether the mean of the dose response changes or drops too far below 1, in which case the displayed dose would have been corrected to a too low value. Table 5.10 shows the mean and the standard deviation of the three groups. For all methods the dose response after the correction still falls within one standard deviation of the ideal dose response. This is especially important for the routine cards, where no significant residual dose is present and therefore only the zero-dose in the order of several μGy has to be removed.

Method	All	Defect	Routine
none	1.0 ± 0.2	1.1 ± 0.5	1.01 ± 0.06
Reread	1.0 ± 0.05	0.97 ± 0.05	1.00 ± 0.05
Linear	1.0 ± 0.05	0.97 ± 0.05	1.00 ± 0.05
Exponential	0.99 ± 0.05	0.97 ± 0.05	1.00 ± 0.05

Table 5.10.: Mean and standard deviation of the dose response before and after residual dose correction for the three different methods and card groups.

The overall quality of all three methods is roughly of the same order. A significant improvement can be reached particularly for the defect cards with a high residual dose where the difference to the ideal dose response decreases to approximately 10 % of the uncorrected value. But also the measurements of the routine cards are improved to about 80 %. Figure 5.24 shows the dose response before a method for residual correction is applied. Most of the cards with a too high dose response are defect cards (marked with a red circle). The improvement of the dose response after the residual dose is corrected with the simple reread method is show in figure 5.25. Particularly striking is the improvement of several defect cards with a very high residual dose and a low irradiated dose of 200 μGy. With an uncorrected dose response of nearly 5, the correction with the simple reread method manages to decrease this deviation to the level of normal cards with a negligible residual dose and a dose response only slightly greater than one.

In conclusion, the simple reread and the linear method yield similar results, with the latter requiring an additional reread, which makes it more time-consuming to apply. The exponential method yields better results in general and for routine cards in particular but fares slightly worse when looking at the defect cards. With the large number of rereads necessary it is much more time-consuming than the simple reread method, but allows on one hand to estimate the amount of rereads necessary to erase the card and on the other hand to predict the residual dose of future measurements. Thus, after one time consuming initial measurement further measurements are no more extensive than the simple reread method with a simple counter for the card allowing the calculation of the respective residual dose.

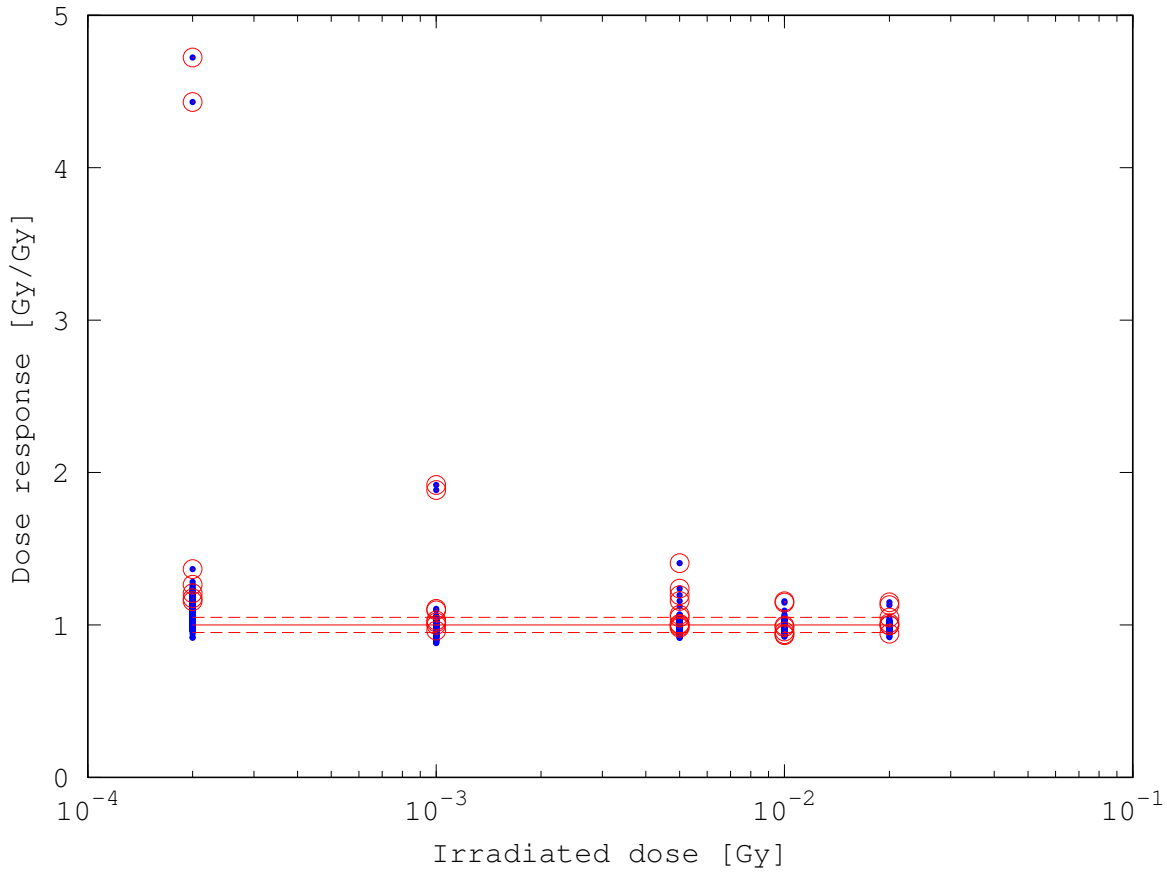

Figure 5.24.: Dose response before residual dose correction with the simple reread method. Defect cards are marked with a red circle, the dashed red line marks the ±5% threshold where most of the dose responses should lie. Notable are two cards at a dose of 200 μGy that have a dose response of nearly 5. After a residual dose correction the result displayed in figure 5.25 is obtained, where no card has a dose response higher than approximately 1.25.

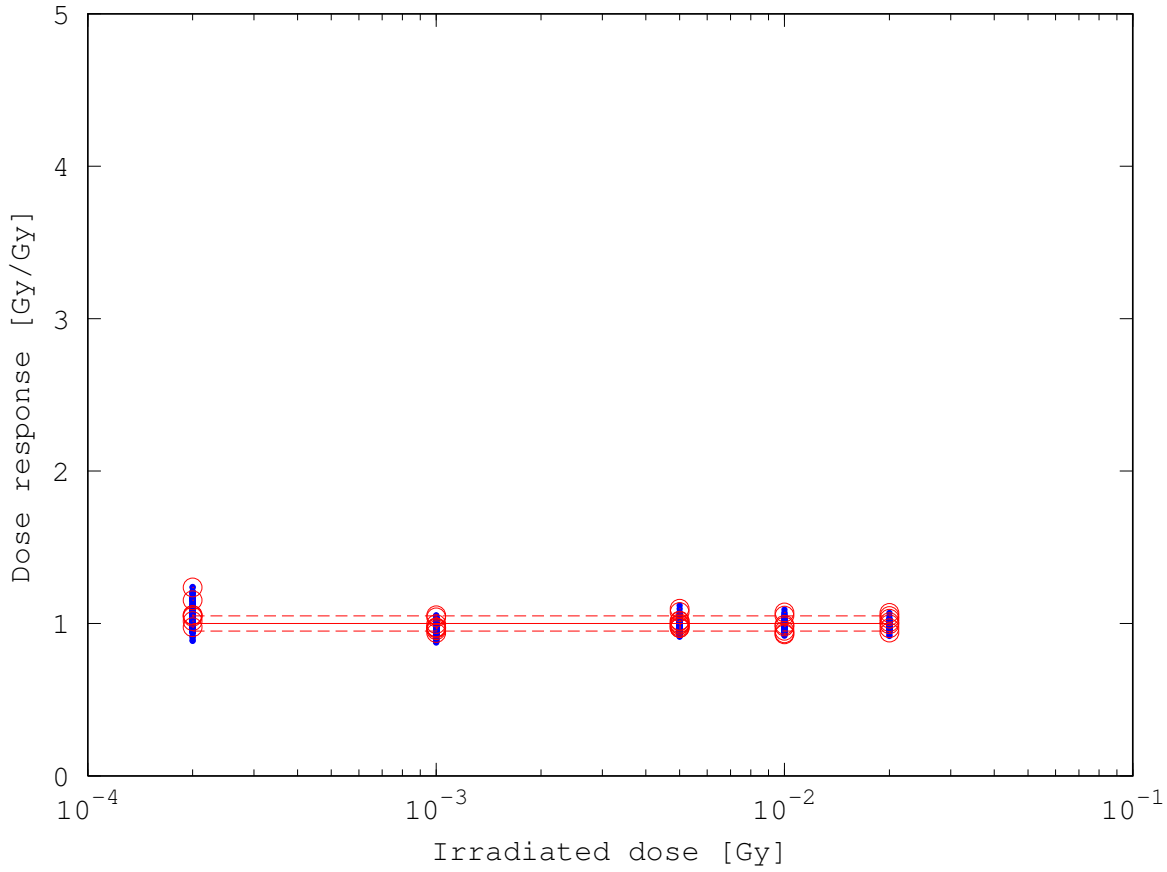

Figure 5.25.: Dose response after residual dose correction with the simple reread method. Defect cards are marked with a red circle, the dashed red line marks the ±5% threshold where most of the dose responses should lie. Note that the outliers visible in the uncorrected dose response plot (figure 5.24) have vanished.

5.5. Long-term Calibration Cards

The calibration cards used in the routine dosimetry programme in Seibersdorf were used for a long-term evaluation (see section 4.6). These cards are irradiated with 5 mGy roughly every two months and subsequently read out. The aim is to investigate a possible long-term effect on the residual dose caused by a large number of medium dose irradiations. The possible buildup was evaluated on the basis of the second readout. The measurements spread out over the course of 10 years and include a total number of readouts per card varying between 61 and 84 (which is between 1 and 1.4 readouts per 2 months) carried out on 1070 different cards.

A simple linear fit was done according to equation 5.11:

$$D_{RR} = A + B \cdot n_{irr} \tag{5.11}$$

Here, D_{RR} is the measured dose of the reread in μGy, A the (theoretical) reread of a new card in μGy and B the increase of the reread per irradiation, in μGy/irradiation.

The linear fit yields the following values for the parameters (table 5.11):

A =	(22.1 $\pm$ 0.3) μGy
B =	(0.035$\pm$0.006) μGy/irradiation

Table 5.11.: Fitting parameters of the long-term calibration cards.

An increase of 0.035 μGy per irradiation is of course too small to be discerned by comparing two consecutive irradiations. Over the course of 100 calibration procedures this would sum up to 3.5 μGy or close to 16% of the original dose of the reread. As the reread of a card can be seen as an estimate of the card specific residual dose, this increase of the reread corresponds to an increase in the residual dose.

Therefore, it is necessary to correct for the individual background not only when very high doses are read out, but also when cards are frequently irradiated with intermediate doses. This also makes a calculation of the increase depending on the accumulated irradiated dose possible. Then parameter A of the linear model remains the same while parameter B can be redefined to correspond to the increase of the reread depending on the accumulated irradiated dose in μGy/Gy. These alternative parameters are given in table 5.12.

A =	(21.5 $\pm$ 0.3) μGy
B =	(11$\pm$2) μGy/Gy

Table 5.12.: Alternative fitting parameters of the long-term calibration cards.

An accumulated irradiated dose of 1 Gy increases the residual dose by (11$\pm$2) μGy. As seen in the section treating different methods of residual dose correction, a one-time irradiated dose of 1 Gy increases the reread to several mGy in only one step. The estimation of the long-term increase of the residual dose is therefore only applicable to accumulated doses composed of single doses in the order of several mGy.

6. Conclusion

Thermoluminescence dosimetry is more and more replacing other techniques of dose measurement, such as film badge dosimetry. The small size, easy production, quick readout process and wide range of measurable doses are among the advantages. However, thermoluminescent materials have some disadvantages:

1. Some materials, LiF:Mg,Ti among them, exhibit supralinear behaviour at high doses. This means that for incident doses exceeding a certain threshold a disproportionately high dose is measured.

2. Every crystal has a slightly different zero-dose, caused by differences in the production conditions.

3. High irradiations lead to a high residual dose imprinted on the crystal.

The aim of this study was the investigation of these problems with a focus on the thermoluminescence dosimeter TLD-100, which is used by the Seibersdorf Labor GmbH as a routine dosimeter. It is made of the thermoluminescent material lithium fluoride doped with magnesium and titanium (LiF:Mg,Ti).

For the first problem a correction function (see section 5.3) has been found, based on a quadratic dependence of the measured on the irradiated dose for doses greater than 0.8 Gy. This is in accordance with literature, but can only be applied to this specific dosimeter setting. Different dosimetry systems (dosimeter and the corresponding reader) with probably a different material have a different supralinear behaviour, if any at all, and the correction function has to be determined anew.

The second problem is already partly accounted for by calibrating the cards. Through this calibration slight differences in the production are usually corrected by a card specific calibration factor.

The third problem is of great importance for all cards, as a residual dose is always present, though it can be small enough to be of no relevance. In any case, a correction of the residual dose can greatly improve the accuracy of a TLD system. The correction can be done either by removing the residual dose or by subtracting an appropriate amount from the determined dose. In the case of the TLD-100 used in this thesis this was tried by several methods, all of which significantly improve the measurements (see section 5.4).

The first method, and the easiest to apply, uses two consecutive readouts. The first readout yields the irradiated dose, which (after all factors earlier determined in a calibration are applied) still might be inaccurate due to a high residual dose. The second readout has been found to be approximately the residual dose imprinted on the crystal during the first readout. The correction is then done by simple subtracting the second readout from the first.

A more complex method uses an exponential decay function to model the decrease of the residual dose depending in the number of readouts. Several preliminary readouts are necessary to fit the parameters of the function. Once this is done the residual dose of a measurement is known and can be subtracted to yield the correct irradiated dose. Additionally, the knowledge of the exponential decay of the residual dose allows to calculate a number of readouts after which the residual dose has fallen below a set threshold. This threshold can, for example, be set to a level at which the residual dose is very low and thus only insignificantly influences the measurement.

The correction from both methods is qualitatively roughly equivalent. The exponential method yields slightly better results, at the expense that more readouts are necessary to obtain the exponential decay function, but with the additional bonus that it is possible to give an estimate of the number of readouts necessary to restore the crystal to a low residual dose.

Through the correction of the residual dose by any of the methods, measurements, especially at low doses, can be significantly improved. As radiation protection should always be designed so as to minimise the radiation workers are exposed to, dosimeters should in the ideal case only record a low dose from the natural background. This is true for the majority of cards, therefore a residual dose correction would improve the measurements of a large number of cards.

In the routine dosimetry service at Seibersdorf, in which the dose readout is done for several hundred cards in one run and several thousand dosimeters are read out every month, a quick and easy to introduce residual dose correction would be the reread method described above.

A. Abbreviations

DEL	Seibersdorf Dosimetry Laboratory
Gy	Gray
HTTL	High Temperature Thermoluminescence
ICRP	International Commission on Radiological Protection
ICRU	International Commission on Radiation Units and Measurements
IEC	International Electrotechnical Commission
LNT	Linear No-Threshold
PIF	Panoramic Irradiation Facility
RIF	Reference Irradiation Facility
TL	Thermoluminescence
TLD	Thermoluminescence Dosimetry or Thermoluminescence Dosimeter
TTP	Time Temperature Profile
TU	Teletherapy Unit
Sv	Sievert
UNSCEAR	United Nations Scientific Committee on the Effects of Atomic Radiation

B. Bibliography

Akkreditierung Austria (2015a). Accredited Bodies for Calibration. Lists of Conformity Assessment Bodies accredited by the Austrian National Accreditation Body.

Akkreditierung Austria (2015b). Accredited Bodies for Testing and Inspection. Lists of Conformity Assessment Bodies accredited by the Austrian National Accreditation Body.

Bos, A. J. J. (2001). High sensitivity thermoluminescence dosimetry. *Nuclear Instruments & Methods in Physics Research, Section B: Beam Interactions with Materials and Atoms*, 184:3–28.

Bos, A. J. J., Vijverberg, R. N. M., Piters, T. M., and McKeever, S. W. S. (1992). Effects of cooling and heating rate on trapping parameters in LiF:Mg,Ti crystals. *Journal of Physics D: Applied Physics*, 25:1249–1257.

Boyle, R. (1664). *Experiments and considerations touching colours*.

Bradbury, M. H. and Lilley, E. (1977). Precipitation reactions in thermoluminescent dosimetry crystals (TLD-100). *Journal of Physics D: Applied Physics*, 10(9):1261.

Bundesministerium für Land- und Forstwirtschaft, Umwelt und Wasserwirtschaft, Österreich (2012). Allgemeine Strahlenschutzverordung. BGBl II 2006/191.

Chen, R. and Fogel, G. (1993). Supralinearity in Thermoluminescence Revisited. *Radiation Protection Dosimetry*, 47(1-4):23–26.

Chen, R. and McKeever, S. W. S. (1997). *Theory of Thermoluminescence and Related Phenomena*. World Scientific, London.

Fairchild, R. G., Mattern, P. L., Lengweiler, K., and Levy, P. W. (1978). Thermoluminescence of lif tld-100: Glow-curve kinetics. *Journal of Applied Physics*, 49:4523.

Garlick, G. F. J. and Gibson, A. F. (1948). The electron trap mechanism of luminescence in sulphide and silicate phosphors. *Proceedings of the Physical Society*, 60(6):574.

Horowitz, Y. S. (1981). The theoretical and microdosimetric basis of thermoluminescence and applications to dosimetry. *Physics in medicine and biology*, 26(5):765–824.

Horowitz, Y. S., Mahajna, S., Rosenkrantz, M., and Yossian, D. (1996). Unified theory of gamma and heavy charged particle tl supralinearity: the track/defect interactioin model. *Radiation Protection Dosimetry*, 65(1-4):7–12.

Horowitz, Y. S. and Moscovitch, M. (2012). Highlights and pitfalls of 20 years of application of computerised glow curve analysis to thermoluminescence research and dosimetry. *Radiation protection dosimetry*, 153(1):1–22.

Horowitz, Y. S. and Yossian, D. (1995). Computerised Glow Curve Deconvolution: Application to Thermoluminescence Dosimetry. *Radiation protection dosimetry*, 60(1):1–114.

Internation Commission on Radiological Protection (2007a). 2007 Recommendations of the International Commission on Radiological Protection. ICRP Publication 103.

Internation Commission on Radiological Protection (2007b). 2012 ICRP Statement on Tissue Reactions/Early and Late Effects of Radiation in Normal Tissues and Organs - Threshold Doses for Tissue Reactions in a Radiation Protection Context. ICRP Publication 118.

International Comission on Radiation Units and Measurements (1993). Quantities and units in radiation protection dosimetry. ICRU Report 51.

International Comission on Radiation Units and Measurements (2011). Fundamental quantities and units for ionizing radiation. ICRU Report 85.

International Electrotechnical Comission (2005). Radiation protection instrumentation - Measurement of personal dose equivalent $H_p(10)$ and $H_p(0.07)$ for X, gamma, neutron and beta radiations - Direct reading personal dose equivalent meters and monitors. International Standard IEC 61526.

International Electrotechnical Comission (2006). Thermoluminescence dosimetry systems for personal and environmental monitoring. International Standard IEC 61066.

International Electrotechnical Comission (2007). Radiation protection instrumentation - Passive integrating dosimetry systems for environmental and personal monitoring. International Standard IEC 62387-1.

Krieger, H. (2009). *Grundlagen der Strahlungsphysik und des Strahlenschutzes*. Vieweg+Teubner, Wiesbaden.

Lavon, A., Eliyahu, I., Oster, L., and Horowitz, Y. S. (2015). The modified unified interaction model: incorporation of dose-dependent localised recombination. *Radiation Protection Dosimetry*, 163(3):362–372.

Mason, E. W., McKinlay, A. F., and Saunders, D. (1977). The re-estimation of absorbed doses of less than 1 rad measured with lithium fluoride thermoluminescent dosemeters. *Physics in Medicine and Biology*, 22(1):29–35.

May, C. E. and Partridge, J. A. (1964). Thermoluminescent Kinetics of Alpha-Irradiated Alkali Halides. *The Journal of Chemical Physics*, 40:1401.

McKeever, S. W. S. and Lilley, E. (1982). Evidence for trimer formation during dopole clustering in Mg doped LiF. *Journal of Physics and Chemistry of Solids*, 43(9):885–893.

McKeever, S. W. S., Moscovitch, M., and Townsend, P. D. (1995). *Thermoluminescence Dosimetry Materials: Properties and Uses*. Nuclear Technology Publishing, Ashford.

McKinlay, A. F. (1981). *Thermoluminescence Dosimetry*. Adam Hilger, Bristol.

Mische, E. and McKeever, S. (1989). Mechanisms of supralinearity in lithium fluoride thermoluminescence dosemeters. *Radiation protection dosimetry*, 29(3):159–175.

Morehead, F. F. and Daniels, F. (1952). Storage of radiation energy in crystalline lithium fluoride and metamict minerals. *Journal of Physical Chemistry*, 56(5):546–548.

Moscovitch, M., Szalanczy, W., Bruml, W. W., Velbeck, K. J., and Tawil, R. A. (1990). A tld system based on gas heating with linear time-temperature profile. *Radiation Protection Dosimetry*, 34(1-4):361–364.

Oster, L. and Horowitz, Y. S. S. (2010). Investigation of the optical absorption characteristics of slow-cooled LiF:Mg,Ti (TLD-100). *Radiation Measurements*, 45:347–349.

Pagonis, V., Kitis, G., and Furetta, C. (2006). *Numerical and Practical Exercises in Thermoluminescence*. Springer, New York.

Randall, J. T. and Wilkins, M. H. F. (1945a). Phosphorescence and Electron Traps. I. The Study of Trap Distributions. *Proceedings of the Royal Society of London. Series A, Mathematical and Physical Sciences.*, 184(999):365–389.

Randall, J. T. and Wilkins, M. H. F. (1945b). Phosphorescence and Electron Traps. II. The Interpretation of Long-Period Phosphorescence. *Proceedings of the Royal Society of London. Series A, Mathematical and Physical Sciences.*, 184(999):390–407.

Rat der Europäischen Union (2013). Richtlinie des Rates zur Festlegung grundlegender Sicherheitsnormen für den Schutz vor den Gefahren einer Exposition gegenüber ionisierender Strahlung. 2013/59/EURATOM.

Stadtmann, H. (2001). Dose quantities in radiation protection and dosemeter calibration. *Radiation Protection Dosimetry*, 96(1-3):21–26.

Stadtmann, H., Delgado, A., and Gómez-Ros, J. M. (2002). Study of Real Heating Profiles in Routine TLD Readout: Influences of Temperature Lags and Non-linearities in the Heating Profiles on the Glow Curve Shape. *Radiation Protection Dosimetry*, 101(1-4):141–144.

Stadtmann, H., Hranitzky, C., and Brasik, N. (2006). Study of real time temperature profiles in routine TLD read out–influences of detector thickness and heating rate on glow curve shape. *Radiation Protection Dosimetry*, 119(1-4):310–313.

Stoebe, T. G. and DeWerd, L. A. (1985). Role of hydroxide impurities in the thermoluminescent behavior of lithium fluoride. *Journal of Applied Physics*, 57:2217.

Strutt, J. E. and Lilley, E. (1981). Kinetics of clustering and precipitation in LiF doped with MgF_2. *Journal of Physics and Chemistry of Solids*, 42(9):827–836.

Thermo Fisher Scientific Inc. (2007). *Product Overview - Materials and Assemblies for Thermoluminescence Dosimetry*.

TLD Poland (2015). TLD Poland - Products. `http://www.tld.com.pl/tld/products.html`. Accessed 15.2.2015.

UNSCEAR (2008). Sources and Effects of Ionizing Radiation. UNSCEAR 2008 Report, United Nations Scientific Committee on the Effects of Atomic Radiation.

Wachter, W. (1982). New method fot he optimization of thermoluminescence sensitivity. *Journal of Applied Physics*, 53:5210.

Wiedemann, E. and Schmidt, G. C. (1895). Über Lumineszenz. *Annalen der Physik und Chemie*, 54:604–625.